2009-01-01

Aluminum Hydride Compunds: A Theoretical and Experimental Spectroscopic Study

Layra E. Reza
University of Texas at El Paso, lereza@miners.utep.edu

ALUMINUM HYDRIDE COMPOUNDS: A THEORETICAL AND EXPERIMENTAL SPECTROSCOPIC STUDY

LAYRA E. REZA

College of Engineering

Department of Mechanical Engineering

APPROVED:

_____
Felicia Manciu, Ph.D., Chair

_____
Ahsan R. Choudhuri, Ph.D.

_____
Arturo Bronson, Ph.D.

_____
Patricia D. Witherspoon, Ph.D.
Dean of the Graduate School

ALUMINUM HYDRIDE COMPOUNDS: A THEORETICAL AND EXPERIMENTAL SPECTROSCOPIC STUDY

By

LAYRA E. REZA, B.S.

THESIS

Presented to the Faculty of the Graduate School of

The University of Texas at El Paso

in Partial Fulfillment

of the Requirements

for the Degree of

MASTER OF SCIENCE

Department of Mechanical Engineering

THE UNIVERSITY OF TEXAS AT EL PASO

August 2009

Acknowledgements

First, I would like to thank my research advisor, Dr. Felicia Manciu. Not only has she been the most supportive and wonderful advisor, but she has been a great friend. Words cannot express the gratitude I feel towards her for all the help and support she has given me. I would like to thank her specially for always believing in me and for taking me back as a graduate student. At a very difficult moment in my life, she was there for me. I will never forget what she has done for me, and without her advice this thesis would not have been possible.

I would like to thank my committee members Dr. Choudhuri and Dr. Bronson for letting me be part of this research project and for welcoming me into the Mechanical Engineering department. I also would like to thank them for their time and critique of this work. Also, I would like to thank the other members of Dr. Manciu's lab, Jay, Young, Luis, and Dr. Durrer for making this journey enjoyable.

Finally, I would like to thank my family for all the support they have given me. My mom and sister for always being willing to listen to me and to provide encouraging words. I thank them and my dad for their unconditional love. Particularly, I would like to thank my amazing common law husband for being so supportive. He never grew tired of my complaints and was always ready to give me comforting words of support. Thank you for your patience and for taking care of me.

Table of Contents

List of Tables

List of Figures

Chapter 1

Introduction

1.1. *Introductory remarks*

Recently, given its reputation as a high energy density fuel, aluminum hydride has received renewed interest as a material that is particularly suited for rocket propulsion. For example, aluminum hydrides have 10% hydrogen by weight, and a hydrogen density of 0.148 g H_2/cm^3 which is twice that of liquid hydrogen[1, 2]. Its high hydrogen content and its highly exothermic combustion, which are advantageous characteristics for any propellant compound, and the combination of metal oxidation and low molecular weight, make aluminum hydride an excellent candidate for rocket propulsion, especially in upper-stage motors, where low weight is most desirable[3].

Furthermore, it has been predicted that replacing aluminum with aluminum hydride (alane) will result in a 10% gain in specific impulse of about 20 seconds over currently used aluminum propellants[2,3]. Such an increase in optimum performance is possible because of this metal hydride fuel's low ignition temperature of 1450 K and low combustion temperature of 3391 K. Indeed alane has an increased burning rate as compared with that of pure aluminum, which ignites at around the alumina melting point and combusts at 3716 K.[2]

However, the utilization of aluminum hydride presents several disadvantages: (i) the colorless solid material reacts violently with water and atmospheric moisture[4], (ii) it has low chemical and thermal stability, and (iii) it is sensitive to friction[2]. Its instability in air causes its structure to change over time[5], with generation of excessive amounts of hydrogen gas during storage[6]. It is believed that the layered structure of this material is the reason for the release of H_2 gas[7]. On the other hand, the formation of a thin protective oxide layer surrounding the alane particles allows a slow down of the material decomposition, rendering the compound kinetically stable[8]. It is also known that the equilibrium hydrogen pressure at room temperature required to form a thermodynamically stable alane compound is greater than 0.7 GPa[9].

Therefore, it is desirable to design synthesis methods that could slow down the decomposition rate of this material, creating a final product which would have a longer storage lifetime and could be handled without extreme precautions; these being preferred properties of any solid propellant. Since reviews of known synthesis methods, and of structural, thermodynamic, and combustion characteristics of aluminum hydride can provide insights into the nature of this unique material, as well as a strong basis for future research, they are presented below.

Currently, there are seven known phases of aluminum hydrides; these are α', δ, ε, ξ, ß, γ, and α-AlH_3 phases. All of these are described below in conjunction with a variety of other aluminum hydride compounds, such as Al_2H_6 and Al_4H_6.

1.2. Chemical Synthesis Methods

The most common method employed for aluminum hydride synthesis is the chemical one. This type of synthesis will also produce the most stable form of all known aluminum hydride compounds, i.*e.* alane or AlH_3.

Aluminum trihydride dates back to 1947, when it was first synthesized by Finholt *et al.*[10]. However, back then the chemical approach produced an alane etherate complex, which was unstable in solution, and it precipitated after synthesis. Any attempt to desolvate the complex resulted in decomposition of the material to the original reactants, *e.g.* aluminum and hydrogen. The lack of stability arose from polymerization of the hydride. Later, in 1968, Bower *et al.* [11] successfully synthesized non-solvated alane in six different crystalline phases. It is interesting to note that all six phases exhibited different physical characteristics.

More importantly, the Bower *et al.* [11] method allowed, for the first time, the synthesis of a stable phase of non-solvated aluminum hydride, *i.e.* α-AlH_3.
The method involved the reaction of lithium aluminum hydride ($LiAlH_4$), aluminum chloride ($AlCl_3$), and diethyl ether ($(C_2H_5)_2O$, as the solvent) in the following manner:

$$3\,LiAlH_4 + AlCl_3 \xrightarrow{(C_2H_5)_2O} 4\,AlH_3Et_2O + 3\,LiCl$$

The reaction products were etherated aluminum hydride and LiCl as precipitates. Also, an excess of $LiAlH_4$ was necessary, so that the ether could be removed without causing alane decomposition. This was the most difficult problem

encountered since the decomposition of the sample occurs around the same temperature as the solvent desorption[1]. Later in the process, contaminants such as lithium chloride were removed by washing the final product in ether.

This chemical method requires a heating treatment to promote the evolution of various metastable phases to the most stable α-AlH_3 phase. For example, ß and γ-AlH_3 convert after a heating treatment of 65°C for 7 hours. Also, the presence of lithium borohydride ($LiBH_4$) during heating enhances the conversion of metastable phases to the α-AlH_3 phase.

The synthesis proceeded as follows:

AlH_3 etherate + $LiAlH_4$/$LiBH_4$ + heating ⟶ γ-AlH_3 → ß-AlH_3 + further heating ⟶ α-AlH_3

Excluding $LiBH_4$ from the heating process and applying a heat treatment of 60°C for 4 hours resulted in the synthesis of another phase, γ-AlH_3, alone. Similarly, the α'-AlH_3 phase was prepared by heating the alane etherate for about 70 hours at 40°C; again, without the presence of $LiBH_4$ [12]. In contrast, the ß-AlH_3 phase was only obtained in conjunction with other phases. Two of the other phases, δ-AlH_3 and ε-AlH_3, were formed when water was present during the crystallization process, while ξ-AlH_3 was formed when crystallization took place in di-n-propyl ether. The α'-, δ-, ε-, and ξ-AlH_3 phases do not convert to the α-AlH_3 phase. In addition to these

crystallites, seed crystals of α-AlH_3 were nucleated by introducing an alane feed solution into a refluxing ether-benzene solution of $LiBH_4$ and $LiAlH_4$ at 79°C [11].

In the last five years, new methods designed to stabilize this compound have been formulated. In 2003, Petrie *et al.*[13] stabilized alane by treating it with an acidic solution, which contains a stabilizing agent such as an electron donor, an electron acceptor, or a compound to coordinate the Al ion. Also, Petrie *et al.*[13] modified the previous chemical method by adding an excess of toluene to the filtration step, as well as sodium borohydride. The resulting diethyl ether-toluene solution was heated and distilled to reduce the amount of ether in the solution, until a precipitate formed. This precipitate was washed and then added to an acidic solution, to dissolve and remove all contaminants, until pure α-AlH_3 was obtained. The authors stated that the final product was more stable than that produced by Bower *et al.*[11].

Another modification to the Bower *et al.*[11] method was used by Yartis *et al.*[8] They produced solid γ-AlH_3 by heating the alane etherate in a mixture of ether and benzene. The heated solution was distilled of the mixed solvent until the hydride started to crystallize at around 75°C.

1.3. Other Synthesis Methods

In 1965, Appel et al.[14], tried to produce aluminum hydride by hydrogen-ion bombardment. An aluminum disk of 99.999% purity was carefully cut into the

desired dimensions, annealed at very high temperatures, and washed with a high concentration of acid. Subsequently, the disk was mounted in a cyclotron beam line and bombarded with highly energetic deuterons. However, this procedure has many drawbacks. For example, following the bombardment, the disk was found to be radioactive. An x-ray diffraction (XRD) indicated an hexagonal structure, which was determined to be that of aluminum hydride in its most stable phase, but the procedure only produced a hydride with a very small percentage of hydrogen.

In 1993, a laser ablation method was employed by Chertihin *et al.*[15] to produce various aluminum hydride compounds. This synthesis method consisted in mounting an Al target on a rod, which was rotating at 1 rpm, while focusing and applying a 10 ns pulse with an Nd:Yag laser at 30-50 mJ/pulse of laser power. A mixture of H_2 and Ar gases was allowed to flow through the system as the aluminum atoms were deposited. The concentration of Al atoms in the gas phase was found to be around 0.2 %. The basic process in these experiments is to permit thermally activated Al atoms to react with H_2 gas before being quenched and condensed in an Ar atmosphere. The reaction products were further identified by means of infrared analysis to be AlH, AlH_2, and AlH_3.

A decade later, Wang *et al.*[16] using, again, a laser ablation procedure and infrared analysis observed formation of the following hydrides: AlH_2, AlH_3, Al_2H_2, Al_2H_4, and Al_2H_6. However, this group used only pure H_2 as the gas present during synthesis. The main difference between the experimental results obtained by Wang *et al.*[16] as compared to Chertihin *et al.*[15] is the successful formation of the compound

Al_2H_6. Wang *et al.*[16] attributed the hydride formation to: (i) the pure H_2 atmosphere caused the formation of a large amount of AlH_3, (ii) the large amount of AlH_3 synthesized permitted hydrogen diffusion, and consequently, the dimerization of polymeric solid trihydride $(AlH_3)_n$ into Al_2H_6 by an exothermic reaction. Also, as reported by this group, the formation of solid aluminum hydride Al_2H_6 occurred during the evaporation of the hydrogen matrix, which allowed for the association of individual molecules.

Most recently, in 2007, a completely different approach was followed by Xi *et al.*[17] for producing a new stable cluster of these hydrides, *i.e.* Al_4H_6, which was predicted to have stability similar to that of boranes. In this study, a pulse discharge procedure was used to generate various aluminum hydride ions, which were later analyzed by mass spectroscopy. Aluminum metal was vaporized in the presence of an excess of hydrogen atoms, while being cooled by helium. More specifically, an aluminum electrode was struck with a discharge, while plasma containing hydrogen atoms, formed by the dissociation of H_2 gas, expanded down within the container being used while at the same time reacting and forming ionic clusters. The final products were analyzed by means of a mass spectrometer. The new complex was found to have a highest occupied molecular orbital–lowest unoccupied molecular (HOMO-LUMO) gap of 1.9 eV. As suggested by the authors, the large energy gap implies a highly stable compound. Thus, if the anionic species of $Al_4H_6^-$ can be stabilized to solid Al_4H_6, it may have an exothermic reactive energy

greater than a mixture of Al and Al_2H_3. This valuable characteristic of this new material will raise its status to that of the most powerful solid rocket propellant.

1.4. Crystal Structure

According to Bower *et al.*[11], microscopic investigations of the α-AlH_3 phase reveal a hexagonal and a cubic structure. Meanwhile, the γ-AlH_3 phase displays bundles of fused needles. Similarly, the α'-AlH_3 phase contains small multiple needles that appear to be growing from a common point. In contrast, the etherated phase appears as translucent spherical precipitates.

More specifically, α-AlH_3 has a C_{3v} symmetry[7] and it also belongs to the R3c space group with eight atoms per primitive cell. The hexagonal structure was found to be the most stable for a=4.94Å and c=11.80Å. This structure is formed by alternating planes of aluminum and hydrogen atoms stacked perpendicular to the c-axis[7]. Therefore, each of the aluminum atoms is octahedrally surrounded by six hydrogen atoms, three in the plane above and three in the plane below. These vertex-sharing AlH_6 octahedral building blocks are connected by three dimensional networks of Al-H-Al bridging bonds which are consistent with the high density of the crystal[8]. Two other possible crystal structures, *i.e.* cubic and orthorhombic, were reported by Ke *et al.*[5] by employing density functional theory. The authors also reported that these structures were more stable than the hexagonal one.

In contrast to α-AlH_3, the γ-AlH_3 which was synthesized by Yartis *et al.*[8] exhibited an orthorhombic unit cell with a=5.38 Å, b=7.35Å, and c=5.77Å. The similarity of the γ-AlH_3 structure with that of the α-AlH_3 consists in the AlH_6 octahedral blocks, but differs in the blocks connectivity. For the γ-AlH_3 phase, the prominent feature is the existence of two different types of Al-2H-Al bridging bonds. This type of bonding forms large cavities between AlH_6 octahedrons, which are responsible for the much smaller (by 11 %) density of this unstable polymorph[8].

Xi *et al.*[17] reported that the aluminum atom framework for Al_4H_6 is a distorted tetrahedron with a terminal hydrogen atom bonded to each aluminum atom, while two hydrogen atoms form bridging bonds across two aluminum atoms. These two sets of bridging bonds are three-centered. The bonding of Al_4H_6 resembles that of boranes.

The foregoing studies on aluminum hydrides demonstrate the polymorphic structures, and consequentially, different properties. However, the viability of the Al_4H_6 is still in a developing stage, consisting of primarily a simulation of possible molecular structure. The exact determination of the Al_4H_6 structure awaits its experimental synthesis as well as its production in significant quantities.

1.5. Theoretical studies of Aluminum Hydrides

The literature contains an appreciable amount of theoretical studies regarding α-AlH_3. However, given the complexity of this material, a consensus has

still not been reached and more calculations are necessary to elucidate various aspects concerning other phases of these types of hydride compounds. For example, Rao *et al.*[18], through ab-initio calculations, determined that both AlH_3 and Al_2H_6 posses the characteristics of magical clusters and relative inertness, *i.e.* unwillingness to either accept or donate an electron. They also found AlH_3 to be the most stable cluster in the AlH_n series, due to its having the highest ionization potential. Their calculations showed that AlH gains energy as Al attaches to an H atom. A different behavior was revealed for AlH_2, where a decrease in energy was obtained. Finally, the ionization energy of Al suggests that AlH_3 is the most stable configuration.

The formation of AlH_4 is unlikely, given that two of the hydrogen atoms would remain molecular and would bind only weakly with the AlH_2 cluster. However, if the two hydrogen atoms form bridging sites with the appropriate aluminum atoms, the Al_2H_6 cluster structure could be created, a structure similar to that of diborane. Therefore, the stability of the Al_2H_6 cluster was attributed to the hydrogen bridging bonds and to the Al-Al bonds formed. Rao *et al.*[18] also found, in the case of Al_2H_6 cluster, a slightly negative net charge on the hydrogen atoms, which is consistent with the interaction between metals and hydrogen; the charge transfer consisted of $Al^{+0.15}$ $H^{-0.05}$. However, since this transfer was very small, they determined the bond to be mostly covalent.

Yartis *et al.*[8] computed the structure of the γ-AlH_3 phase, and reported that it exhibits large cavities between AlH_6 octahedra as compared to the α-AlH_3 phase,

which explains the smaller density of the former. Furthermore, they found that the decomposition enthalpy of γ-AlH_3 was lower than that of the α-AlH_3 phase. If the decomposition is truly reversible indicating the enthalpy of formation, their finding implies that the binding energy of the γ-AlH_3 phase is lower, rendering it less stable.

Ke *et al.*[5] calculated that the decomposition reactions of α-AlH_3, in hexagonal, cubic, and orthorhombic forms, were endothermic. Even though the polymorphs were unstable, they could still be stabilized kinetically. Also, a very slow decomposition rate was predicted for temperatures less than 373 K. The free energies of formation were found to be positive, which suggests that the hydride would decompose. Also, because of the negative value of the enthalpy of formation, the decomposition was reported as endothermic. In conclusion, these types of hydrides can be stored for some time.

Sandrock *et al.*[19], investigating the decomposition of alane, found results similar to those reported by Ke *et al.*[5]. They stated that for thermodynamic reasons the following reaction is highly favorable and not easily reversed[19]

$$AlH_3 \rightarrow Al + {}^{3}/_{2}\, H_2$$

While alane was reported as being metastable at room temperature, they found that it can be easily handled in an inert gas or under vacuum, without decomposition. They attributed this stability to an alumina layer at the surface of the compound, a layer that acted as a kinetic barrier and encapsulated the

hydrogen-based material. However, for temperatures around 60-200°C, decomposition was inevitable.

More detailed calculations were performed by Ismail and Hawkins[6] which calculated an enthalpy of formation of -11.4 kJ/mol, absolute entropy of 30 kJ/mol°C, and Gibbs free energy of formation of 45.4 kJ/mol. Again, these calculations show that, thermodynamically, alane should decompose to yield aluminum metal and hydrogen gas. Also, they showed experimentally that the thermal stability can be enhanced by increasing the particle size for alane. Therefore, they propose a model of decomposition, which occurs when the sample is heated at 60°C, a temperature that causes a 7.5% weight loss, or the formation of aluminum crystals.

More specifically, Ismail *et al.*[5] proposed a nucleation and growth mechanism for AlH_3 decomposition. Alane particles decompose on the surface at nucleating sites accelerating to a two-dimensional growth of the Al phase. The Al phase grows inwardly to the core of the particle, though the decomposition slows as a result of the formation of Al_2O_3.

Another similar study done by Kato *et al.*[20] showed that the thermal decomposition of AlH_3-etherate begins with an endothermic reaction at 350 K when it desolvates into γ-AlH_3 which has an Al-H bonding similar to that of the etherate. The desolvating step is characterized by a weight loss of 31.5 mass%. Also, in a subsequent step they found that the γ-AlH_3 unstable phase transformed exothermically into α-AlH_3 at temperatures above 373 K. Finally, again by an

endothermic dehydriding reaction at temperatures above 405 K, they found that the compound exhibited another 6.5% weight loss, similar to the one reported by Ismail *et al.*[6].

1.6. Combustion Characteristics

For aluminum hydride to replace aluminum as a solid rocket fuel additive, a comparison of the burning characteristics of Al and alane is needed. An advantage of aluminum hydrides is that they have 10% hydrogen by weight, and a hydrogen density of 0.148 g H_2/cm^3, which is twice that of liquid hydrogen[1,2]. Such high hydrogen content and low molecular weight indicate that aluminum hydride is an ideal substance for rocket propulsion. In 2007, DeLuca *et al.*[2] proposed a two step mechanism regarding combustion of this material as follows:

1) Dehydrogenation $AlH_3 \rightarrow Al + {}^3/_2\ H_2$

2) Oxidation $Al + {}^3/_4\ O_2 \rightarrow {}^1/_2\ Al_2O_3$

Dehydrogenated alane burns at elevated pressures and temperatures with combustion times and temperatures similar to those observed for pure aluminum particles. Furthermore, rapidly dehydrogenizing alane in a propellant would release hydrogen gas very close to the burning surface. Therefore, the hydrogen gas would burn in the primary flame zone. As a consequence of step one, the remaining aluminum would ignite and burn as usual. Following step two, a considerable

amount of heat would be released, though passivation does occur as a result of Al_2O_3 formation.

Thus, when alane is added to solid propellant formulations, it will enhance rocket performance by increasing specific impulse[1]. This affirmation is based on the following considerations. According to DeLuca *et al.*[2], by replacing aluminum with alane, a lower combustion temperature is obtained, as well as a lower percentage of combustion products. Thus, the lower throat erosion will increase the average specific impulse.

A similar study was conducted by Bazyn *et al.*[3], where alane was burned in a shock tube at a temperature of 2650 K and a pressure of 8.5 atm. Their conclusions were mostly in agreement with those established by DeLuca *et al.*[2], namely that replacing aluminum with alane will result in a release of hydrogen near the surface of the solid, which will also burn with the oxidizer. However, they concluded that under test conditions, the dehydrogenation step is completed before the incident shock reaches the end of the combustion chamber wall, in about 100 μs. Consequently, the particles that burn behind the reflected shock are mostly aluminum.

Although not established yet, the combustion of other aluminum hydride compounds, such as the latest predicted Al_4H_6 complex, appears to be endowed with very promising properties. For example, the predicted heat of combustion of Al_4H_6 to Al_2O_3 and water is 438 kcal/mol[17]. This is about three times greater than that of

methane, which makes this complex a great potential candidate for rocket fuel applications.

1.7. Concluding remarks

It is worth noting that although successful alane production was achieved several decades ago, to this date, a complete understanding of aluminum hydrides has not been yet achieved. As previously mentioned, due to their various physical and thermodynamic properties, these high energy complexes show promise as rocket fuel materials.

However, as revealed by the above literature review, there are major obstacles in the road to practical application of these types of materials, namely their low stability under normal conditions. Furthermore, the lack of experimental results is a direct indication of the difficulty of controlling these complexes. Fortunately, during the past years new approaches to synthesis have been proposed in the quest for a stable compound. Therefore, pursuing this goal, we employed different synthesis routes in conjunction with several spectroscopic characterization techniques to shed some new light on this old material.

Chapter 2

Experimental Details

2.1 Introduction

The various samples investigated in this work were synthesized by two different procedures. First, aluminum hydride (alane) was synthesized following the method of Bower *et al.*[11] and Schmidt *et al.*[4], which allows for production of non-solvated alane, especially the most stable α-AlH_3 phase. This method involves the reaction of lithium aluminum hydride ($LiAlH_4$) with aluminum chloride ($AlCl_3$) reagents in a diethyl ether $(C_2H_5)_2O$ solvent[11]:

$$3\,LiAlH_4 + AlCl_3 \xrightarrow{(C_2H_5)_2O} 4\,AlH_3Et_2O + 3\,LiCl$$

The reaction products were etherated aluminum hydride and LiCl precipitates. The unwanted excess of $LiAlH_4$ reagent, as well as the ether solvent, was subsequently removed by washing, without causing decomposition of the final alane product[11].

It is worth noting that this chemical method requires a heating treatment to promote the evolution of various metastable phases to the most stable α-AlH_3 phase.

Also, the presence of lithium borohydride ($LiBH_4$) during heating enhances the conversion of metastable phases to an α-AlH_3 phase.

The second procedure, which consisted of an attempt to synthesize α-AlH_3 crystals, was made using a method modeled after the synthesis procedures of both Brower *et al.*[11] and Petrie *et al.*[13]. It is similar to that employed earlier in this project, which consisted of preparing a solution of $LiAlH_4$ and $AlCl_3$ with diethyl ether as a solvent. However, there are some differences. For example, according to Petrie *et al.*[13] the presence of an excess of metal hydrides while the solution is subjected to a heating treatment, which is needed for the stabilization of the material, aids in the crystallization procedure of the alane complex as well as in the removal of impurities, especially when any remaining alkali metal chloride is not removed by the filtration procedure. These considerations apply specifically to $LiAlH_4$ and $LiBH_4$. In addition, according to Brower *et al.*[11], once the metastable phase produced in the first part of the synthesis is subjected to heating, the alpha phase can be more easily crystallized in a combined benzene and ether solution than in a pure ether solution, if all the conditions are carefully controlled.

The exact synthesis procedures are described in detail below. The resulting products were analyzed by infrared absorption and Raman spectroscopy techniques. A brief discussion of the theoretical background of these techniques and the experimental set-ups used in the measurements performed in the course of this dissertation are also presented in this chapter.

2.2. Chemical Synthesis of Aluminum Hydride

2.2.1. Preparation method for α-AlH_3

According to Schmidt *et al.*[4], to obtain a pure sample, purified reagents, minimal exposure to light, and higher heating temperature are necessary to decrease the alane decomposition. Therefore, to carry out the synthesis in a water and oxygen free atmosphere, purified nitrogen gas provided by a chemical synthesis Schlenk line was used. Furthermore, the precursor materials were purchased anhydrous, and, as an extra precaution, the anhydrous ether was allowed to react with metallic sodium overnight, and then further distilled to remove any existing moisture. A nitrogen filled dry box was used for the preparation of all precursor materials and for the storage of the resultant alane.

First, in a dry box, two three-necked flasks were filled with 1.3 g of $AlCl_3$ and 1.5 g of $LiAlH_4$. One neck was fitted with a N_2 connector, while the rest were sealed with rubber stoppers. The flasks were then transported to the Schlenk line, where nitrogen was allowed to flow through the connector. After an increase in the N_2 flow, the stoppers were exchanged with condensers and additional funnels. The system was purged again with N_2 to remove any contamination.

The next step consisted in preparing a 1.0 M ether solution of both $AlCl_3$ (10 mL, 0.01 mol) and $LiAlH_4$ (40 mL, 0.04 mol). The reactions being highly exothermic, before adding the ether, a cold bath at -5°C was placed around to the flasks. This

procedure was performed using a Dewar flask with liquid N_2 and acetone. Then, 10 mL of ether was injected into the addition funnel of the flask containing $AlCl_3$ in a dropwise manner and under heavy stirring. The same procedure was followed to introduce 40 mL of ether into the flask containing $LiAlH_4$. Meanwhile, the temperature of the cold bath was monitored and stabilized at the desired -5°C.

After the two precursors were completely dissolved, the two reactions were combined and immediately filtered. For the required filtering procedure, inside the dry box, a flask equipped with a N_2 connector was filled with 0.2 g $LiBH_4$ and connected right away to the filtering set-up that was attached to the Schlenk line. The removal of the $AlCl_3$-$(C_2H_5)_2O$ solution (with a syringe) was performed under increased N_2 flow. Also, the addition funnel was replaced with a rubber stopper and the system immediately purged of any contaminants. The $AlCl_3$-$(C_2H_5)_2O$ solution was then injected into the flask containing $LiAlH_4$-$(C_2H_5)_2O$ solution by opening the funnel very slowly and starting a dropwise addition under heavy stirring. After the reaction of the two solutions, a filtering procedure was again applied. In this case, a hollow wire was connected between the flask and the filtering set-up, and under a pressure difference created by a vacuum in the new empty flask, the solid LiCl was filtered from the etherated alane. The etherated alane was subsequently mixed with the $LiBH_4$ under heavy stirring.

To start the transformation of the metastable alane to the stable α-AlH_3 phase, a heat treatment at ~ 65°C was applied for 12 hours using a hot oil bath. Given that the final product, *i.e.* non-solvated α-AlH_3, is not soluble in ether, while

any precursor still left in the solid is, the washing step was performed using ether. Thus, 24 mL of ether was injected into the solid, and the solution was stirred for 10 minutes. The solvent with impurities was again removed under vacuum and the non-solvated α-AlH_3 was allowed to dry overnight. Finally, to protect the final product from atmospheric moisture and to minimize the light exposure, the flask was covered with aluminum foil and left inside the dry box.

2.2.2. Continuous batch crystallization method for α-AlH_3

Similarly to the previous procedure due to the high reactivity of both the precursors and the end material regarding atmospheric conditions, the preparation was again carried out either under a nitrogen atmosphere or under vacuum provided by a chemical synthesis Schlenk line. In addition, all the precursors used were purchased anhydrous, and, as an extra precaution, the anhydrous ether was allowed to react with metallic sodium overnight and then further distilled to remove any existing moisture.

The first step consisted of reacting two metal hydrides with $AlCl_3$ in diethyl ether to form the desired aluminum hydride product along with some extra by-products. In a glove box, one three-necked flask was filled with 3.0 g of $AlCl_3$, while two 20mL glass vials were each filled with 1.8 g of $LiAlH_4$ and $LiBH_4$, respectively. The flask was sealed with rubber stoppers. The precursors were then transported to the Schlenk line, where a condenser fitted with a nitrogen connector was connected

to the flask containing the $AlCl_3$, while nitrogen was allowed to flow through the connector.

The next step consisted in preparing an ether solution of $AlCl_3$, LiAlH4 and $LiBH_4$. Given the high exothermic nature of this reaction, the flask was surrounded by a cold bath at -10°C. This procedure was performed using a Dewar flask with liquid N_2 and acetone. Then, two injections of 30 mL of ether each were added through a stopper in the flask containing $AlCl_3$, rapidly and under heavy stirring. Meanwhile, the temperature of the cold bath was monitored and stabilized at the desired -10°C. Then, under a positive flow of N_2 through the condenser and with an external flow of N_2, with the aid of a funnel, contents of the two vials of alkali metal hydride were added through one of the necks. An additional 30 mL of ether was added to aid in the mixing of the solution.

After the three precursors were completely dissolved, the reaction was stirred for an additional 30 minutes. For the required filtering procedure, a three-necked flask was attached to the Schlenk line through a funnel filter containing a silicate and equipped with a N_2 line. The alane etherate complex was then transferred through a hollow wire between the flask and the filtering set-up. At this point, 20 mL of benzene was injected into the filter to aid in removing any solution that was stuck in the walls of the filter. According to Petrie *et al.*[13], at this stage a large excess of an aromatic organic solvent, in this case benzene, should be introduced into the filtrate to aid in the removal of any impurities still left in solution. Then,

after byproducts were completely filtered, an additional 40 mL of benzene were added to the solvated alane through one of the stoppers.

The next step consisted in removing some of the solvent through the Schlenk line and into a N_2 filled trap by decreasing the pressure with the aid of the vacuum line. Immediately after the solvent started to evaporate, a white precipitate started to form around the walls of the flask. Part of the solvent was left in solution, and an aliquot of the solvent and precipitate mixture was removed at this stage. This aliquot was analyzed by means of Infrared and Raman spectroscopy. To the remaining solution, two $LiAlH_4$ pellets were added; however, they did not dissolve. Then, the solution was filtered again and transferred to a single necked flask fitted with a N_2 connector. The filter was removed and replaced with a plastic stopper while maintaining a positive N_2 flow to avoid any contamination.

At this point, the solution consists of the unstable α'-AlH_3 phase, which needs to be subjected to a slow heating process in order to convert most of this mixture into the stable alpha phase, and to simultaneously start the crystallization process. Following a similar procedure outlined by Petrie *et al.*[13], the first step in creating crystals of alane is to distill the ether-benzene solution to reduce the amount of ether, and a distillation column should be used. This process should be performed while heating the solution under vacuum and until a precipitate is obtained. Two slow heating treatments are recommended, the first at a temperature of around 82-85°C for about two hours, while the second heating treatment should last between 20-40 minutes at around 90-93 °C.

To start the transformation of the metastable alane to the stable α-AlH_3 phase, a heat treatment at ~ 90°C was applied for around 3 hours using a hot oil bath under a N_2 atmosphere. After the heating treatment was stopped, the solution was allowed to cool. At this point, the solution appeared partially contaminated, as some of the mixture turned from white to gray. The next step consisted in injecting an additional 20 mL of ether and 50 mL of benzene into the solution to try to remove the impurities from the mixture. After this solvent was allowed to mix with the old solution under heavy stirring, the plastic stopper was replaced with a fractionating column. Then, an additional 70 mL of benzene and 20 mL of ether were added to the solution. This mixture was heavily stirred for 15 minutes. Then, a second heat treatment was applied for around one hour at ~ 90°C. After the heat treatment was stopped, the solution was allowed to cool for about 20 minutes. At this point, most of the ether had been removed from solution. The fractionating column was then replaced with a plastic stopper while another filtering setup was prepared. Then, with a positive N_2 flow, the solution was transferred to a new flask through a hollow wire. All of the mixture that was contaminated (a gray solution) was removed by the filter in this step. Meanwhile, the receiving flask contained a white precipitate that covered the wall. This flask was stored in a dry box for further examination of this precipitate.

The filtered product remaining in the new flask was left under vacuum for around one hour to remove any benzene and/or ether still present in the precipitate.

The final dry product was sealed under N_2 and transferred to a dry box to avoid contamination and/or decomposition of the material.

2.3. Experimental techniques and set-up

2.3.1. Introductory theoretical background

Fourier transform infrared (FT-IR) and Raman (FT-Raman) spectroscopy are two powerful characterization techniques that provide information regarding the chemical nature and structural properties of the bonding between atoms. Both of these two techniques are mainly concerned with the interaction of electromagnetic radiation and the molecular vibrational and rotational levels of the molecular structure and major chemical functional groups in a material[21]. For some vibrational modes, only a small number of atoms have large displacement, while the rest do not participate in the vibration. In this case, the frequency of these modes is characteristic of these specific atoms, independent of the other atoms in the molecule. Thus, these specific features represent a specific chemical group that is present[21]. Still, every material has different vibrational modes from all other materials; this allows spectroscopic techniques to accurately identify and characterize different materials.

Most important is the fact that these two techniques focus on two different mechanisms of photon energy transfer that affect both the molecular structure and

symmetry characteristics of the sample being observed. Therefore, they give complementary information that provides the ability to look at all active vibrational and rotational levels of molecules. There are three types of effects that occur when a sample is irradiated by electromagnetic radiation; the energy can be transmitted, absorbed or scattered. FTIR is concerned with the first two while FT-Raman is concerned with the latter.

Infrared absorption occurs when a sample is irradiated by a stream of photons of different energies and the molecule absorbs this energy and increases the energy of its vibrational state. The molecule is able to absorb only certain characteristic frequencies that match its natural vibrational states. In general, the changes in configuration and orientation of a molecule due to vibrations and rotations after absorption of a stream of photons correspond to energy of a few tens of meV, which correspond to the infrared region of the electromagnetic spectrum; this corresponds to the $10^4 – 10^2$ cm^{-1} frequency range. While the frequency depends on the particular vibrational state, the intensity of the absorption depends on the effectiveness of the transfer of energy between the photon and the molecule, which in infrared spectroscopy is dictated by the change in the dipole moment occurring in the molecule as a result of the vibration[22]. A simple dipole moment is defined as the charge in the dipole times the spacing between opposite charges:

$$p = q * d$$

If the molecule analyzed consists of many atoms, *q* can be taken as either the total positive or negative charge present, and *d* can be defined as the distance between

the “centers of gravity” of the positive and negative charge clouds[22]. The change of dipole moment occurs when the electric field of the photon acts to exert forces in opposite directions on the negative and positive centers of the molecule. The nature of these opposite forces is what causes the distance, *d*, between the centers of opposite charges to change which gives rise to a dipole moment that will oscillate with the frequency of the photon.

This implies that the molecule during vibration should not have a center of symmetry so that the electric field can move atoms with excess opposite charges in different directions; therefore, vibrations that are antisymmetric with respect to their centers of charges are infrared active.

As mentioned before, when an electric field interacts with a molecule it induces a dipole moment. This induced dipole moment and the electric field are related by a property called polarizability as follows:

$$p = \alpha * E$$

This property is a measure of the deformability of the electron cloud of the molecule by the electric field[22]. The dipole moment is a vector while the polarizability is described by a tensor. It is also important to note that for a vibration to be Raman active it must occur with a change in the polarizability of the molecule. The change in polarizability gives rise to amplitude modulation, at certain frequencies, of the induced dipole moment oscillation, which give rise to the Raman frequency components[22].

In summary, the selection rules are as follows: (i) chemical groups that are asymmetric in their molecular structure and undergo a large change in electric dipole during molecular vibration, tend to display strong infrared lines; (ii) materials that are symmetric in their molecular structure and undergo a large change in electron polarizability during vibration, tend to exhibit strong Raman lines.

A description of the properties of alane by both spectroscopic techniques leads to valuable information as revealed in Chapter 3, where a comprehensive analysis is provided for the experimental results obtained. But first, a detailed explanation of the set-up of these two techniques is given below.

2.3.2. Fourier Transform Infrared Spectroscopy

In contrast to other spectroscopic techniques, Fourier Transform Infrared absorption spectroscopy (FTIR) is a non-dispersive technique. This means that different frequencies are not directly separated out spatially, but instead a signal (an interference pattern) is generated vs. the distance travelled by a moving mirror; this permits frequency separation by means of a Fourier transform computation. A Fourier transform spectroscopic system consists therefore of two distinct subsystems; one is the analog optical transducer with input/output optics that allow the interaction of infrared radiation with the sample and the collection of this light into a detector, and the other is the computing system that performs a Fourier

transformation of the interferogram into the desired spectrum, both of which are described next.

The most important component in a Fourier Transform (FT) spectrometer is the interferometer, which is the device for physically analyzing the radiation. Its purpose is to assess the intensity of each wavelength present from the radiation source. The interferometry principle used in an FT instrument is that of the Michelson interferometer, which is schematically presented in Figure 1.

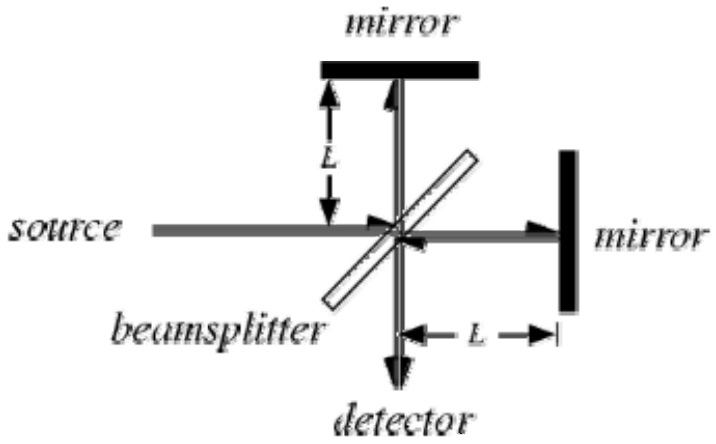

Figure 1: Schematic representation of a Fourier transform instrument[23].

A typical Michelson interferometer consists of four main parts, an infrared source, a beamsplitter, and two plane mirrors, one of which is fixed and a second, which is allowed to move. Parallel infrared radiation emitted from the source travels to the beamsplitter, which is oriented at 45°. Then, the task of the beamsplitter is to divide the light into two beams of equal intensity; one beam will be transmitted and the other reflected. These two beams travel to the two different

mirrors (which are oriented perpendicular to the beam) and are then reflected back to the beamsplitter where they recombine. More specifically, the reflected beam reaches the fixed mirror after traveling a distance L, which is called the *physical distance*. Subsequently, the beam is reflected back to the beamsplitter and returns to it after traveling a distance equal to $2*L$, which is called the *optical path*. The transmitted beam reaches the movable mirror; if this mirror is the same distance from the beamsplitter as the fixed mirror, the beam would have traveled the same physical distance L to reach it. However, as the name implies, the movable mirror travels back and forth around the distance L by an amount equal to δx. When the transmitted beam returns to the beamsplitter, it has traveled a distance of $2(L + \delta x)$. The two beams are recombined at the beamsplitter with an *optical path difference*, also called retardation, of $2*\delta x$.

After the two beams recombine, there are two possible scenarios. The electromagnetic waves combining at the beamsplitter can interfere either constructively or destructively. The type of interference depends on the optical path difference and on the wavelength of the light. The relationship is as follows:

(1) Constructive interference $2*\delta x = n*\lambda$ $n = 1, 2, 3\ldots$

(2) Destructive interference $2*\delta x = (1/2)\ n*\lambda$ $n = 1, 3, 5\ldots$

Consequently, the output beam has an intensity that depends on the amount of constructive interference and thus varies as a function of the optical path

difference and the wavelength of the incident radiation. The intensity is at a maximum when the optical path difference is zero, since all wavelengths of light constructively interfere at this point called the *zero path difference* (ZPD). The plot of detector response as a function of optical path difference is called an interferogram.

The shape of the *interferogram* greatly depends on the characteristics of the light source. For example, the interferogram of a monochromatic source, with only one wavelength, would be a cosine function. The Fourier transform of this interferogram would give a single main peak in the final spectrum. In the case of our broadband source, which has a continuous infinity of wavelengths, the interferogram consists of the sum of all the cosine waves that belong to each distinct wavelength present. For this type of source, only at the ZPD are all of the wavelengths in phase; this is the scenario when the interferogram will show a single maximum and some small peaks close to it. The effects of the chosen beamsplitter (which is a non-ideal crystal), detector response, and of the chosen apodization function (which acts to remove sidelobes in the interferogram) are reflected in the shape of the typical interferogram. Depicted schematically in Figure 2 are the ideal interferogram of a broadband source and the most common interferogram obtained from experiments.

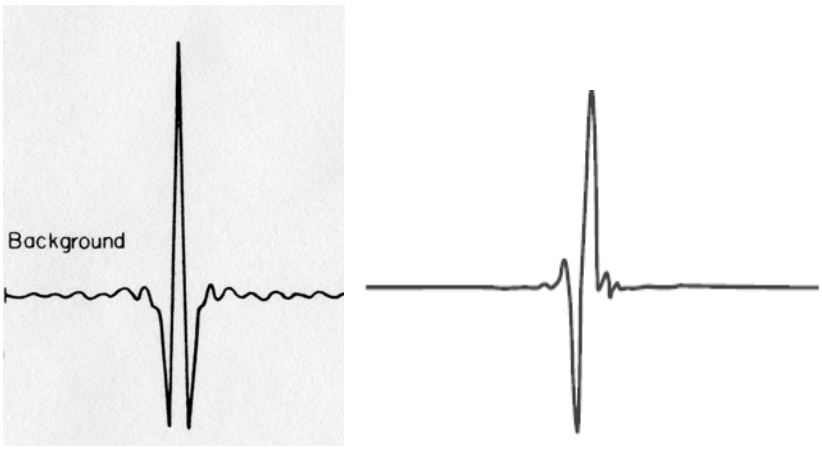

Figure 2: Ideal and experimental obtained interferograms of a broadband source[24].

A common procedure is to allow the movement of the mirror at a constant velocity, so that the interferogram will have a one-to-one linear mapping from the path difference domain (δx) to the time domain (t) via the mirror velocity. This type of interferogram is called a continuous-scan. Thus, the movable mirror in the interferometer can be driven at a constant velocity, which can be chosen between 0.01 cm/s and 4 cm/s. The spectral frequency content then becomes a temporal frequency content at the detector. These frequencies are typically in the range of a few Hz to a few kHz. Also, it should be noted that the chosen velocity of the movable mirror is directly related to the resolution of the data acquisition, since the resolution of an interferometer is determined by the total path difference and varies inversely as the maximum optical path difference[25].

The continuous analog signal forming the interferogram must be integrated after weighting by a cosine function in order to obtain the spectral amplitude. Full Fourier transformation requires many cosine weightings and integration procedures

to be carried out simultaneously in order to recover the entire spectrum. Typically, multiple scans are desired for every sample investigated given that noise in a spectrum is reduced by the square root of the number of scans[22]. However, given that full Fourier transformation is complicated, this cannot be performed in real time, and each interferogram obtained by a single scan is recorded for later processing. Presently, all the recording, weighting by a cosine function, and integration of the analog interferogram signals required by Fourier transform spectroscopy are done with high precision after a previous analog-digital (AD) conversion in a microprocessor.

After having described the main part of an FTIR spectrometer, it is important to explain the other important components of an FTIR spectrometer such as the infrared source, the infrared detector, and the beamsplitter. In this technique the sample is irradiated with a broadband source that is usually a solid material heated by an electric current that acts as a blackbody radiator[22]. Another very important component consists of the detector, the main purpose of which is to measure the infrared energy of the source after it traveled through the spectrometer. Its task is to transform this energy into an electrical signal that can be converted into a spectrum. The most common type is a pyroelectric detector that consists of a ferromagnetic material whose electrical polarization is sensitive to changes in temperature.

In a typical IR transmission or absorption measurement, the outcome is the absorption of the infrared light by the sample as a function of frequency via the

transmitted intensity. Therefore, in order to obtain a reliable transmission or absorption spectrum, two steps should be performed. First, with no sample, a reference background should be taken, which is actually the response of the detector $I_0(\upsilon)$. Second, with the sample in place, another recording of $I_T(\upsilon)$ is taken. When the frequency of the incoming energy matches the frequency of the vibration of the molecules, part of the radiation is absorbed and part is transmitted as is graphically shown in Figure 3.

Figure 3: Schematic representation of incident, reflected, and transmitted light

The relation between the two light beam intensities $I_T(\upsilon)$ and $I_0(\upsilon)$, where the reflection from two sample surfaces (as is true in the case of pellets, which is the form of each of our samples) is neglected, is given by the well known Bouguer-Lambert-Beer law of absorption of light by a partially transmitting medium:

$$I_T(\nu) = I_0(\nu)\, e^{-\alpha(\nu)\, d}$$

where I_0 and I_T denote the intensities of the incident and transmitted beams at a specific wavenumber (ν), α is the liner absorption coefficient at a specific wavenumber, and d is the thickness of the sample. The IR spectrum obtained is

called the transmittance, and is the ratio of $\frac{I_T(\nu)}{I_0(\nu)}$, and is automatically calculated by the computer.

The absorption/transmission spectrum can be obtained in three different regions of the infrared radiation, depending on the properties of the sample that need analyzing. The three regions are:

i) Near Infrared (NIR) from 12500 to 4000 cm^{-1},

ii) Mid Infrared (MIR) from 4000 to 400 cm^{-1}, and

iii) Far Infrared (FIR) from 400 to 5 cm^{-1}.

A specific light source, detector, and beamsplitter have to be selected for each one of these frequency ranges. In the present work a Globar lamp, which is a silicon carbide rod[22], was used. This specific lamp operates best at a temperature of around 1300 K[21] in the range of 20 cm^{-1} – 10,000 cm^{-1} wavenumbers. Also, a pyroelectric detector, namely a DLATGS (deuterated l-alanine-doped triglycine sulfate) room temperature detector was employed. This detector operates best at 360 cm^{-1} to 12,000 cm^{-1} wavenumbers. and a KBr beamsplitter (370 cm^{-1} – 7500 cm^{-1}) were used. Moreover, all the samples analyzed in this work were prepared as pellets with Potassium Bromide (KBr) as the matrix. Here, a very small percentage of sample material is ground with, then mixed with the KBr, which is then pressed into a thin film with the help of a die and a hydraulic press. KBr is transparent in the region of

interest, and the only precaution that should be observed is to avoid any water contamination, which is done by grinding the matrix as little as possible[22].

2.3.3. Raman Spectroscopy

As previously mentioned, FT-Raman is concerned with the scattering effect of light by molecules. In a Raman spectrometer, a sample is irradiated by a stream of monochromatic photons, with energy usually corresponding to the visible part of the spectrum, after which the scattered light is analyzed. There are two types of scattering events that occur in Raman spectroscopy. The first is called Rayleigh scattering where a molecule interacts elastically with light and no change in vibrational or rotational levels occurs. Here the light is scattered without a change in its energy. Then, there is the Raman Effect where the scattered light has undergone an inelastic interaction with the molecule. As a result the vibrational and/or rotational energy of the molecule are changed; these are the normal modes that are probed in FT-Raman[26]. The change in energy levels occurs by an amount ΔE, which by the conservation of energy principle, causes a change in the energy, and therefore, in the frequency of the scattering photon.

$$\Delta E = h\nu_o - h\nu_f$$

The two scattering processes are schematically explained below in Figure 4.

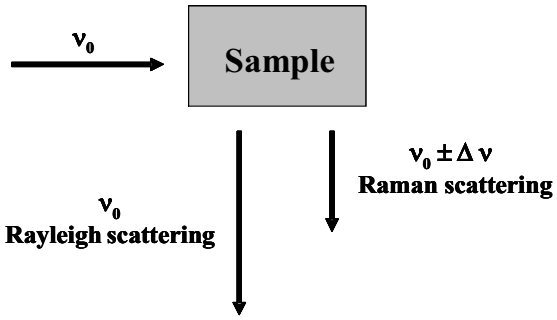

Figure 4: Schematic representation of elastic and inelastic Rayleigh scattering.

There are two possibilities regarding ΔE; it can be positive or negative. The first case occurs when the molecule absorbs energy (ΔE is positive). This is known as the Stokes scattering effect where the scattered photon leaves with a lower frequency (longer wavelength) than the incident radiation. The process is illustrated in Figure 5, where a molecule is in a ground state when it is hit by photons with energy $h\upsilon_0$ and goes into a virtual state. Then, the material goes into a final state that has higher energy than the original while photons with an energy $h(\upsilon_0-\upsilon)$ are scattered.

The second case occurs when the molecule loses some of its energy (ΔE is negative). This is knows as the Anti-Stokes scattering effect where the photon leaves with a higher frequency (shorter wavelength) than the original one. This process is illustrated below, where a molecule is originally in a state other than the ground state; the molecule then gives some of its energy to the incident photons that will be scattered at a higher $h(\upsilon_0+\upsilon)$ energy.

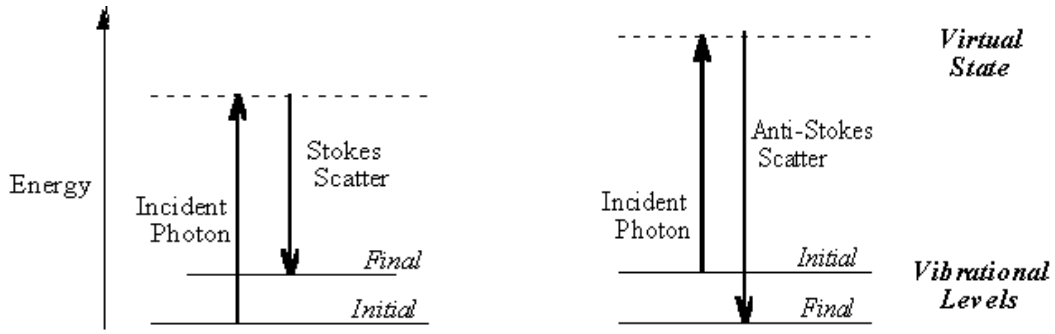

Figure 5: Schematic representation of Stokes and anti-Stokes processes[27].

There is still one problem; elastic scattering (Rayleigh) is much more prominent than inelastic scattering (Raman). For example, only one in 10^8 – 10^{10} photons undergo Raman scattering[22]. Given that, it is very important to have a monochromatic source, which allows selection of a specific wavelength to determine whether the sample undergoes other physical events, such as fluorescence and luminescence. One of the possible solutions is to use a NIR laser; in our case we use a Nd:Yag laser which emits at 1064 nm and which produces a spectrum free of the fluorescence effect.

A Raman spectrum consists of a plot of the intensity of the Raman scattered radiation as a function of its frequency change with respect to the frequency of the incident radiation. This frequency difference is named the Raman shift. Both the Stokes and anti-Stokes shifts are composed of lines, which correspond to vibrations (phonon modes) of the material under investigation. It is important to note that at ordinary temperatures most molecules exist in their ground sate, which implies that the Stokes lines are much more intense than the anti-Stokes lines. This ratio

depends on the temperature of the sample and can be determined from a Boltzmann distribution[22].

2.3.4. Advantages of FT-IR and FT-Raman

There are two very important advantages that make Fourier transform infrared absorption and Raman scattering techniques stand above the dispersive Raman and absorption methods, which employ a monochromator instead of the interferometer used in FT spectrometry. It is important to note that when evaluating different types of spectrometers one must compare the Signal-to-Noise (SNR) ratios. The SNR is a measure of the performance of the instrument and is computed by dividing the peak height of a feature by the average level of the noise. When all else is equal, a greater SNR will tell us which instrument is more sensitive, and consequently, which one will facilitate detecting more features.

The first advantage is called the *Jacquinot's Advantage*, also known as the throughput advantage. Dispersive spectrometers work by focusing a beam of light into the sample, which then goes through a slit, and next into a monochromator that focuses the light into a grating whose main task is to separate the components of polychromatic light by reflecting the radiation through an angle that depends on the wavelength. Then, an exit slit allows only one wavelength at a time to travel outside the monochromator to hit the detector. The grating is rotated to allow the different wavelength elements to exit the monochromator. Different wavelengths

are sequentially permitted to strike the detector, but only for a small amount of time each[28]. Thus, the spectrum is measured one wavelength at a time.

In contrast, an interferometer is designed to allow all the different constituents of light to hit the detector at the same time. This enables irradiation of the sample with high intensity light and no losses, resulting in higher radiation throughput. This advantage results from the fact that an interferometer can have a large circular source at the input or entrance aperture of the instrument without imposing any strong limitation on the resolution (as compared with the entrance and exit slits of a typical grating spectrometer, which must be narrowed to achieve high resolution).

The second advantage is called the *Fellgett's Advantage*, also known as the Multiplex advantage. It is a result of the capability to measure all the available wavelengths simultaneously in an interferometer as opposed to a spectrometer that allows only a selected range of wavelengths. This process is significant in regards to the SNR in various ways. First, for all variables being equal, the SNR of a spectrum from an interferometer is greater than that of a spectrum from a spectrometer by a factor of $M^{1/2}$, where M corresponds to the number of resolution elements[21]. The following example illustrates how M is calculated. Consider a spectrum between 400 cm^{-1} and 4000 cm^{-1}. This spectrum thus has a width of 3600 cm^{-1}. If 4 cm^{-1} is the closest that two peaks in the spectrum can be to each other and still be distinguishable, then the spectrum has a resolution of 4 cm^{-1}. The number of

resolution elements is thus defined by dividing the width of the spectrum by its resolution, which in this case is M = 900.

Also, since the noise is proportional to the square root of the time spent observing every wavelength, the noise in a spectrum from a spectrometer is much greater. This also means that with a spectrometer, a spectrum takes M times longer to acquire as compared to one with the same SNR obtained with an interferometer[28].

Regarding FT-Raman spectroscopy, there is one important difference when compared to conventional Raman Spectroscopy. Most conventional Raman spectrometers use visible lasers, such as the Argon (488 nm) laser, the HeNe (632.8 nm) laser, and diode lasers (785 nm), whereas FT-Raman spectrometers use the Nd:Yag (1064 nm) laser. This is important when considering the fact that the intensity of a Raman line is dependent on the difference between the frequency of the laser and the specific vibration raised to the fourth power, $(v_o - v_i)^4$[21]. This can translate into a decrease of the amplitude of a Raman line of up to a factor of 55 times[21]. This means that either a high-powered laser is needed, which can burn the sample, or that a more sensitive detector is needed. However, very sensitive CCD detectors used in conventional Raman spectroscopy are not suitable for FT-Raman spectroscopy, since their operating range is not useful for the latter application. The solution is either a Germanium or an InGaAs detector in conjunction with a multiplex- measurement (interferometer). Nonetheless, the major advantage of FT-

Raman spectroscopy is the elimination of the noise introduced by the fluorescence effect.

2.3.5. Bruker IFS 66v FT-IR and FRA 106 FT-Raman system

The instrument employed for the infrared experiments performed in this work was a commercial rapid-scan vacuum-based *Bruker IFS 66v* Fourier Transform Infrared Interferometer (FT-IR) with various upgrades. Even though an interferometer does not directly give the desired spectral information, but rather the Fourier transform of the desired intensity vs. frequency, several other advantages, as previously mentioned, have made this system a powerful and widely used one.

A schematic view of the optical path inside the *Bruker IFS 66v* is shown in Figure 6. The *Bruker IFS 66v* is essentially a Michelson type two-beam interferometer. Its basic components are the collimating optics, a fixed mirror, a beamsplitter and a movable mirror. To compensate for imperfections in the mirror movement, the *Bruker IFS 66v* uses a dynamical alignment control system.

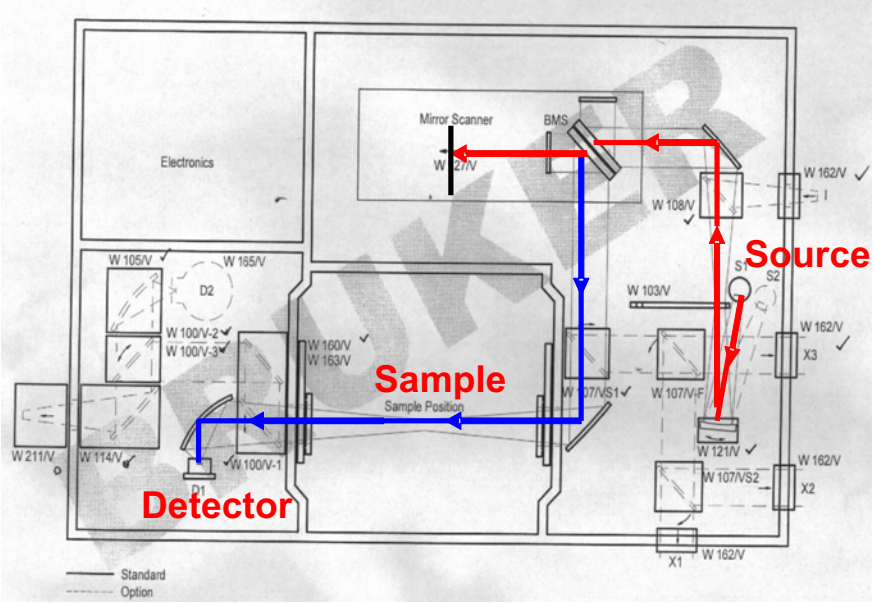

Figure 6: Schematic representation of Bruker IFS 66 v optical path[29].

This control system facilitates the achievement of a proper alignment of the interferometer by using a stabilized single mode Helium-Neon (He-Ne) laser. The He-Ne laser beam follows the same optical path as the infrared light, but passes through its own beamsplitter, which is a reference portion located at the center of the beamsplitter assembly. Since the He-Ne laser beam is a monochromatic light source, its interference fringes occur at constant intervals throughout the range of mirror displacement. Each laser fringe corresponds to a mirror displacement of one-half the laser wavelength, which for a He-Ne laser corresponds to 3164 Angstroms. The signal coming from the He-Ne laser is detected by the corresponding Si photo-diode and analyzed by the electronic circuit that drives the electro-magnetic transducers which control the fixed mirror. Then, by automatically counting fringes, the instrument can obtain a measure of the mirror displacement relative to the ZPD

reference. In this way, any deviations of the fixed mirror can be adjusted to follow those of the moving mirror, resulting in a perfect alignment. This is only one of the features provided by the instrument to make a reliable spectrum possible.

The *Bruker FT-IR IFS 66v* is interfaced directly to a *Bruker FRA 106* FT-Raman system, whose optical path is presented in Figure 7. Computer controlled mirrors select the interferometry in either Raman or infrared mode. The *FRA 106* is attached to the side of the *IFS 66v* interferometer, and utilizes most of the optical components of the interferometer.

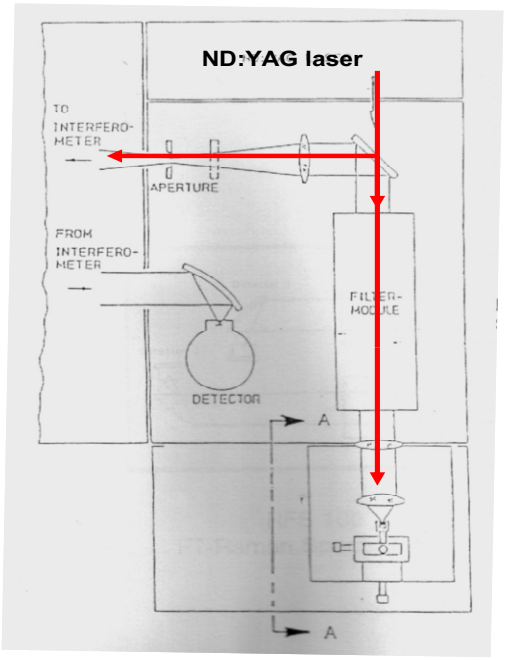

Figure 7: Schematic representation of Bruker FRA 106 optical path[29].

The current FT-Raman measurements were performed with the excitation of an Nd:Yag laser, which is attached to the back of the *FRA 106* instrument.

Chapter 3

Experimental and Theoretical Results

3.1 Introduction

Given the difficulty of preparing a pure and a stable sample of various aluminum hydrides, very little information regarding experimental vibrational modes is available. Most of the known vibrational modes have been determined theoretically. Moreover, most of the studies available concern only the most stable polymorph, α-AlH_3. The first infrared study of aluminum hydride was published in the 1970's, by Schmidt *et al.*[4], who identified two different phases of non-solvated alane synthesized by chemical methods. However, the report did not specify exactly which polymorphs were obtained. Two years later, Matzek *et al.*[12] reported the synthesis of α'-AlH_3 and included an infrared study that matched one of the samples obtained by Schmidt *et al.*[12]. Still, due to the presence of impurities and lack of new synthesis methods, spectroscopic studies of this material were not published for the following two decades.

In 1993, Chertihin *et al.*[15] used the pulsed-laser evaporation method to produce various aluminum hydrides such as AlH_2, AlH_3, and Al_2H_2. Also, at this time, *ab initio* calculations were performed to determine the expected infrared vibrations of the following hydrides AlH, AlH_2, AlH_3, AlH_4, and Al_2H_2. In addition,

density functional theory (DFT) calculations were used for comparison with the experimental values obtained. It was observed that symmetric stretching modes were more energetic than the observed antisymmetric ones. Ten years later, Wang *et al.*[16] conducted laser ablation experiments similar to those of Chertihin *et al.*[15] and found similar vibrational lines for the various aluminum hydrides. Likewise, theoretical calculations by means of DFT yielded results similar to those reported by Chertihin *et al.*[15]

Recently in 2008, Wang *et al.*[30], using DFT, calculated both infrared and Raman vibrations for α-AlH_3 and γ-AlH_3 polymorphs for comparison. Structurally, the main difference between the two polymorphs is the double bridge bond present in the γ-AlH_3 polymorph. However, both polymorphs share a common building element, an AlH_6 octahedron where one Al atom is surrounded by six H atoms. In the α-AlH_3 polymorph, the octahedra are connected by sharing vertices, thereby forming one bridge bond of Al-H-Al. On the other hand, in the γ-AlH_3 polymorph the octahedra are connected by sharing vertices as well as edges, thus forming double bridge bonds of Al-2H-Al.

(a) (b)

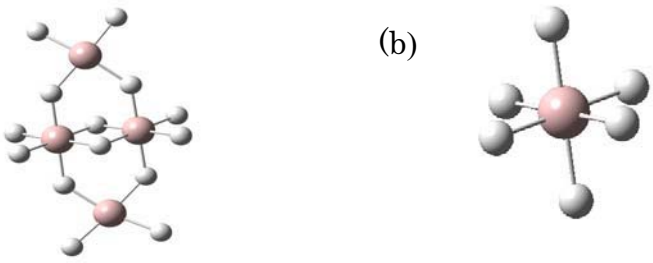

Figure 8: (a) Double bridge bond in γ-AlH_3 (b) Building block in α-AlH_3

The α-AlH_3 polymorph contains 8 atoms per unit cell, while the γ-AlH_3 polymorph contains 24; therefore, more complicated vibrations occur in the latter[30]. Also, it was found that γ-AlH_3 undergoes a fast decomposition into the most stable α-AlH_3 polymorph.

In addition to theoretical calculations some experimental results have been published. Very recently, Wong *et al.*[31] conducted pressure dependence experiments to obtain the vibration modes of the α-AlH_3 polymorph. This highly energetic material is not stable under standard atmospheric conditions, but it is suitable for use at high pressures. Raman spectra of chemically synthesized α-AlH_3 were acquired at various pressures by employing the 514.5 nm excitation wavelength of an argon ion laser at a power of 130 mW. At high pressures, the sample became transparent. Although no decomposition was observed, the sample turned partly grey due to the laser radiation. Additionally, an infrared spectrum at ambient conditions was recorded for comparison with the previous studies. Finally, to determine the number of active vibrational modes, the authors used group theory. They found four Raman and six infrared active modes.

The most recent experimental study was performed in 2008 by Tkacz *et al.*[32]. Raman spectra of both α-AlH_3 and γ-AlH_3 polymorphs prepared following Brower's method[11], were acquired and analyzed. These backscattering Raman measurements were obtained again with an argon ion laser at an incident wavelength of 514.5 nm. However, a much lower power output was employed for the γ-AlH_3 polymorph, given its sensitivity to decomposition. In this study, five major Raman vibrational

lines were observed, which were in good agreement with previously reported experimental results. The most pronounced Raman features obtained in this study were those at 513 and 724 wavenumbers.

This literature review suggests that more comprehensive experimental spectroscopic analyses are needed. Furthermore, accurate investigations of aluminum hydride characteristic vibrational modes can only be achieved after successful preparation of a high quality sample, free of impurities or polymorph mixtures. Consequently, an all-inclusive optical spectroscopic study would be a great benefit and would allow for a straightforward and accurate identification of various polymorphs of this material, based on current knowledge.

3.2 Experimental Results and Analysis

3.2.1 FTIR Analysis

Infrared transmission measurements were carried out with a Bruker IFS 66v spectrometer, equipped with a DTGS detector and a KBr beamsplitter. The samples were prepared in the form of pellets by embedding the desired material in a polycrystalline KBr matrix. An accumulation of 256 scans was performed for each spectrum.

Typical infrared absorption experimental results of the products from the chemical synthesis procedure described in section 2.1.1 are presented in Figure 9.

Due to the expected decomposition of the sample at room temperature and normal pressure, the spectra shown in this figure are recorded at different exposure times, as specified next. Spectrum 9(a) in black represents a freshly synthesized alane sample that has not been exposed to the atmosphere. Meanwhile, the spectra 9(b) in blue and 9(c) in red represent the alane sample after 20 and 40 minutes of atmospheric exposure, respectively. Also, these spectra of the samples are vertically translated for better observation.

The various bands and peaks present in the spectra are assigned as follows. In the spectrum of the sample without atmospheric exposure, 9(a), the most intense peaks at 2223 cm^{-1}, 2289 cm^{-1}, and 2389 cm^{-1} correspond to $LiBH_4$ precursors. The bands around 1125 cm^{-1}, 2939 cm^{-1} and 2979 cm^{-1} are attributed to the solvent used in the sample preparation, diethyl ether, while the broad peak centered around 3400 cm^{-1} is due to water absorption by the sample. The other two vibrational lines present in this sample at 620 cm^{-1} and 1632 cm^{-1} could be assigned to two different materials. According to Matzek et al[12] these vibrations confirm the presence of the stable α-AlH_3. However, these two vibrations occur in the region of vibrations that correspond to Al_2O_3; then, we need more information to adequately assign these two vibrational lines.

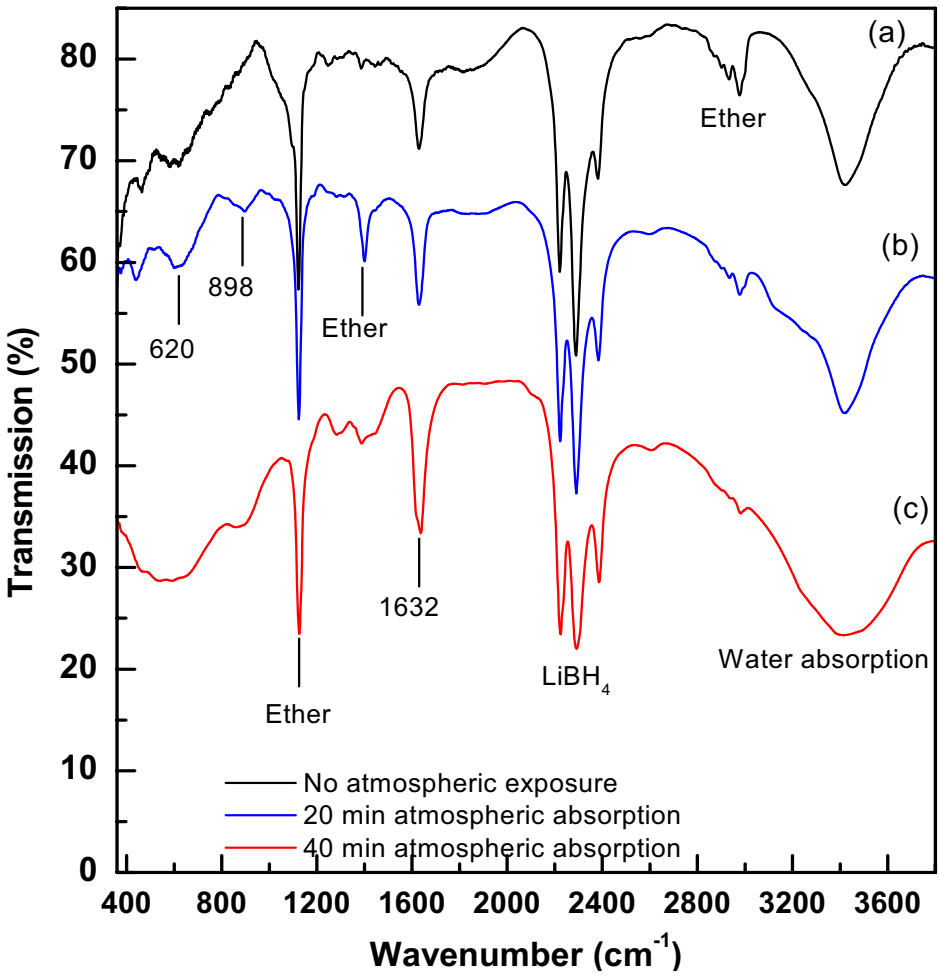

Figure 9. Infrared absorption spectra of alane at different atmospheric exposure times from least (a) to greatest (c). 1st preparation method.

The spectrum of the sample that had been exposed to the atmosphere for approximately 20 minutes, 9(b), also contains the $LiBH_4$ precursor's three vibrational lines at 2223 cm^{-1}, 2289 cm^{-1}, and 2389 cm^{-1}, and those corresponding to the solvent used in the sample preparation. However, while the solvent vibrations at 1125 cm^{-1} and 2979 cm^{-1} are still present in this spectrum, the vibration at 2939 cm^{-1} disappears. Furthermore the existence of new solvent absorption, at 1408 cm^{-1},

could be observed. The broad peak centered around 3400 cm^{-1} representing water absorption is still present. The spectrum of the sample with the greatest atmospheric exposure, 9(c), is almost identical to that of 9(b), with the following exceptions: the solvent vibration at 1408 cm^{-1} splits into two features at 1296 cm^{-1} and 1420 cm^{-1}, features still corresponding to the solvent; and the vibration at 620 cm^{-1} experiences a broadening, being now centered around 572 cm^{-1}.

After identifying the vibrations present in these three spectra, we recognize the following three main differences. First, as expected, as the sample is exposed to the atmosphere for a longer amount of time, the hygroscopic nature of the sample is revealed by the water absorption band, which broadens in a significant manner. Second, the vibrational lines that correspond to diethyl ether either decrease or disappear with time. This is again expected since the solvent is allowed to evaporate as time passes by. Third, a slight modification of the characteristic α-AlH_3 frequencies is observed with longer atmospheric exposure. For the sample with no atmospheric exposure, only two vibrational lines that could be assigned to alane are observed. However, a definite broadening of the 620 cm^{-1} absorption band to lower frequency can be seen for a 40 min exposure time. Given that the wavenumber region in question is associated with Al_2O_3, this observed broadening could reveal the alane oxidation. This effect should be expected since, as previously reported in the literature, the formation of a thin surface alumina layer is likely, a layer that will prevent any further alane decomposition. On the other hand, according to

Matzek et al[12], a fingerprint vibration of α-AlH_3 at 898 cm^{-1}, confirms the presence of the non-decomposed stable hydride, as previously stated.

Given the fact the most intense vibrations in the previous sample were assigned to both the precursor and the solvent, two additional filtering and washing procedures were performed on the sample. The infrared absorption results corresponding to measurements of the sample immediately after two filtering procedures (black line) and after longer atmospheric exposure (blue line) are presented in Figure 10.

Similarly to the spectra in Figure 9, these spectra contain a broad band centered at 3500 cm^{-1} and attributed to water absorption by the sample. Also, these spectra contain the vibrational lines at 613 cm^{-1}, 1623 cm^{-1} that can be assigned either to Al_2O_3 or to α-AlH_3, and the vibration at 881 cm^{-1} that demonstrates the presence of alane. However, there are some clear differences between the two spectra shown in Figure 10, differences pointed out by arrows and revealing the disappearance with time of $LiBH_4$ at 2273 cm^{-1} and of diethyl ether at 1078 cm^{-1} and 2978 cm^{-1}.

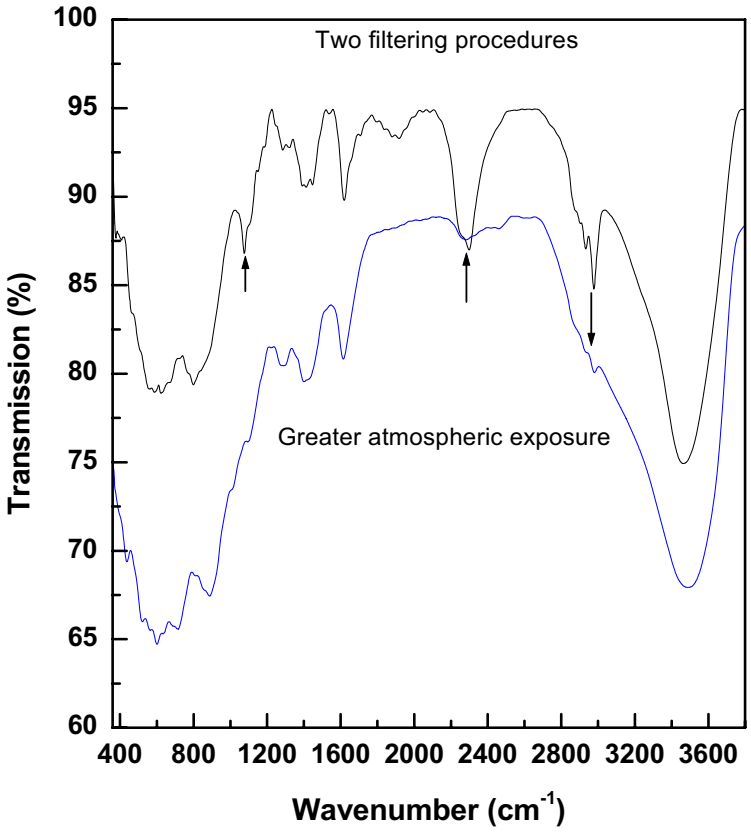

Figure 10. Infrared absorption spectra of the alane after two filtering procedures (black) and after greater atmospheric exposure (blue). 1st preparation method.

To fully determine the effect of the two additional filtering and washing procedures, Figure 11 shows the spectrum of a freshly synthesized sample in black and the spectrum of a sample after two filtering procedures in red. These graphs clearly show, as marked by the arrows, the disappearance of $LiBH_4$ at 2273 cm^{-1} and of diethyl ether at 1078 cm^{-1}, 1407 cm^{-1} and 2978 cm^{-1}.

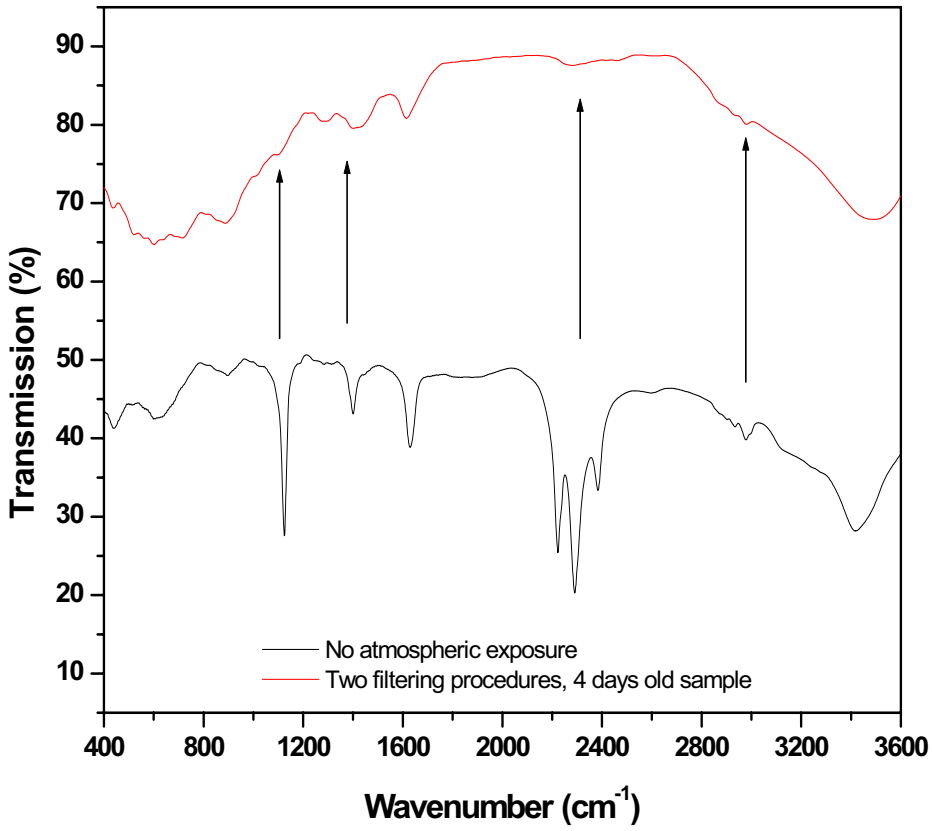

Figure 11. Comparison of the infrared absorption spectra of alane with no atmospheric exposure (black) and after two filtering procedures (red). 1st preparation method.

Therefore, after analyzing these two samples we can conclude that the additional washing procedures successfully remove the unwanted precursor and solvent.

In addition, it is interesting to note that in Figure 11 the spectrum in red corresponding to the sample after two filtering procedures, a sample that is also 4 days old, is significantly changed from that of the freshly synthesized sample. Then, a comparison with Al_2O_3 could give us more information regarding the

decomposition of the sample as time goes by. This comparison is presented in Figure 12, where the spectrum of the 4 days old sample is in black and the spectrum of Al_2O_3 is in red.

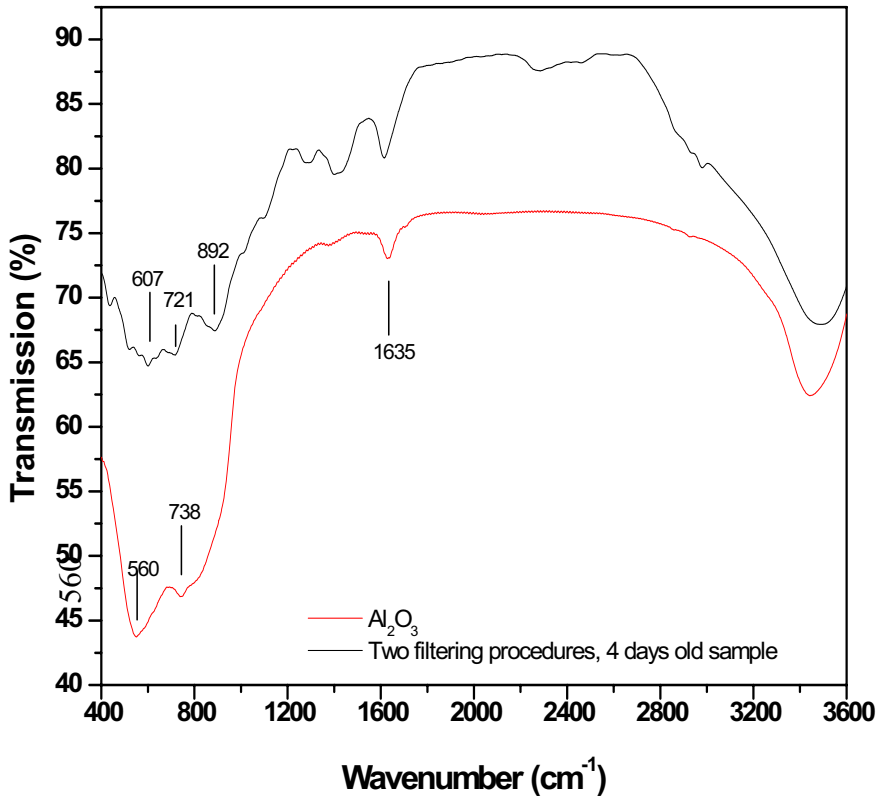

Figure 12. Comparison of the infrared absorption spectra of the alane after two filtering procedures (black) with that of alumina (red). 1st preparation method.

As seen in Figure 12, the three main absorptions of Al_2O_3 occur at 560 and 738 and 1635 wavenumbers, which are broad in nature and coincide with the region where three of the characteristic vibrations of α-AlH_3 occur at 607 and 892 and 1632 wavenumbers. This corroborates our previous assumption that the vibrations at 620 cm^{-1} and 1632 cm^{-1} are not easy to assign to a specific material. However, the

vibration at 892 cm^{-1} can be unambiguously assigned to α-AlH_3. Furthermore, comparison of the 620 and 1632 cm^{-1} absorption band intensities in a spectrum of freshly synthesized alane (please see Figure 9) and in the alumina spectrum (please see Figure 12) reveals the larger intensity of the 1632 cm^{-1} vibrations for the alane sample. Also, as the alane sample gets older the decomposition process is reflected in the increasing intensity of the 620 cm^{-1} absorption, which is the fingerprint of alumina. Then, it can be safe to state that the chemically synthesized sample does contain alane, without excluding the possibility of an oxidation layer forming on the material surface.

Next, let us analyze the alane sample synthesized by the method described in section 2.1.2. The infrared transmission spectra of this sample as a function of exposure time to atmospheric conditions are presented in Figure 13 (black lines). The spectrum labeled 13(a) represents the measurement performed with the least amount of atmospheric exposure and the spectrum labeled 13(c) the data for the greatest amount of atmospheric exposure. The blue line spectrum, 13(d), represents an infrared absorption measurement of the sample after two filtering procedures.

Similarly to the previous results on the sample synthesized by another method, the least atmospheric exposure spectrum of this sample, 13(a), contains diethyl ether vibrations at 1120 cm^{-1}, 1403 cm^{-1}, 2918 cm^{-1}, and 2980 cm^{-1}. As some of the ether is allowed to evaporate, the last two vibrations disappear for the rest of the spectra.

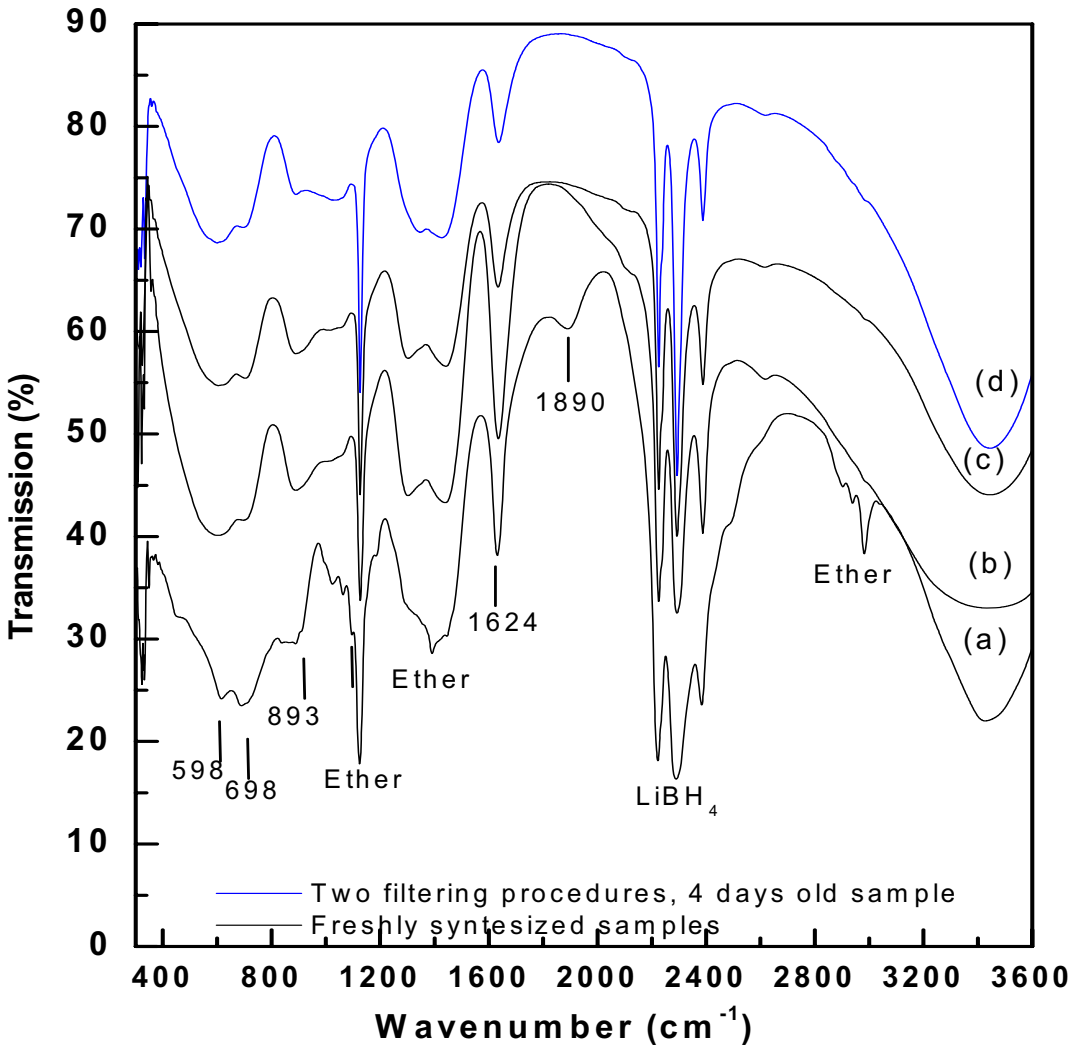

Figure 13. Infrared absorption spectra of freshly synthesized alane (black) and filtered sample (blue). 2nd preparation method.

All four spectra contain three vibrations at 2205 cm^{-1}, 2296 cm^{-1}, 2394 cm^{-1} that correspond to the precursor $LiBH_4$. The vibration at 893 cm^{-1} present in all spectra demonstrates the presence of α-AlH_3. Moreover, the vibration at 1890 cm^{-1} can also be assigned to α-AlH_3 according to Wong et al[31]. Again, for the 1624 cm^{-1}, 698 cm^{-1}, and 607 cm^{-1} vibrations an unambiguous assignment cannot be made,

although, more plausibly, they belong to α-AlH_3 rather than to Al_2O_3, as previously discussed.

The table below summarizes all the currently observed infrared vibrations in comparison with the ones reported in literature.

Table 1. Comparison of main Infrared vibrations present in alane prepared by two different methods with those of alumina and with those obtained in previous studies.

Method 2.1.1	Method 2.1.2	Matzek et al [12]	Al_2O_3
620	607	640	560
	698	680	738
898	893	870	
1632	1624	1650	1625

We can then conclude that the observed vibrations mostly resemble those of the α-AlH_3 phase. However, the presence of Al_2O_3 cannot be ruled out. Moreover, the presence of an oxidation layer as a stabilizer has been discussed before.

Thus, synthesis of the samples by chemical methods results in a material that contains impurities that mainly arise from the precursor's presence. Attempts to remove them lead to enhanced decomposition / oxidation of the aluminum hydride product. The next section consists of an inclusive analysis of Raman spectroscopic data on the same samples.

3.2.2 FT-Raman Analysis

The FT-Raman measurements were performed in backscattering geometry with a Bruker FRA 106 operating with 1064 nm continuous-wave diode-pumped Nd:YAG laser light. A small cavity of an aluminum cup holder was filled with powder or an NMR tube was used for a liquid sample, and then placed at the focus of the excitation laser beam. Again, each spectrum was produced by an accumulation of 256 scans. Also, a fluorescence background subtraction was performed for all spectra.

The experimental Raman result from the liquid sample that was synthesized using the chemical procedure described in section 2.1.1 is presented in Figure 14. The aliquot was withdrawn before exposing the sample to a heating treatment for an extended period of time.

The various bands and peaks present in the spectrum are assigned as follows. The most intense peaks at 2865 cm^{-1}, 2940 cm^{-1}, and 2985 cm^{-1}, and the vibrations at 843 cm^{-1} and 437 cm^{-1} correspond to the diethyl ether solvent used in the sample preparation. As with other peaks observed in the infrared bands, the assignment of the vibration present at 1452 cm^{-1} is debatable. It can be assigned to either diethyl ether, or, according to Kato et al[20], to a different crystalline phase of alane, namely γ-AlH_3. In order to eliminate this uncertainty, we analyze the sample after a heating treatment, which might give us more insight regarding the origin of this vibration.

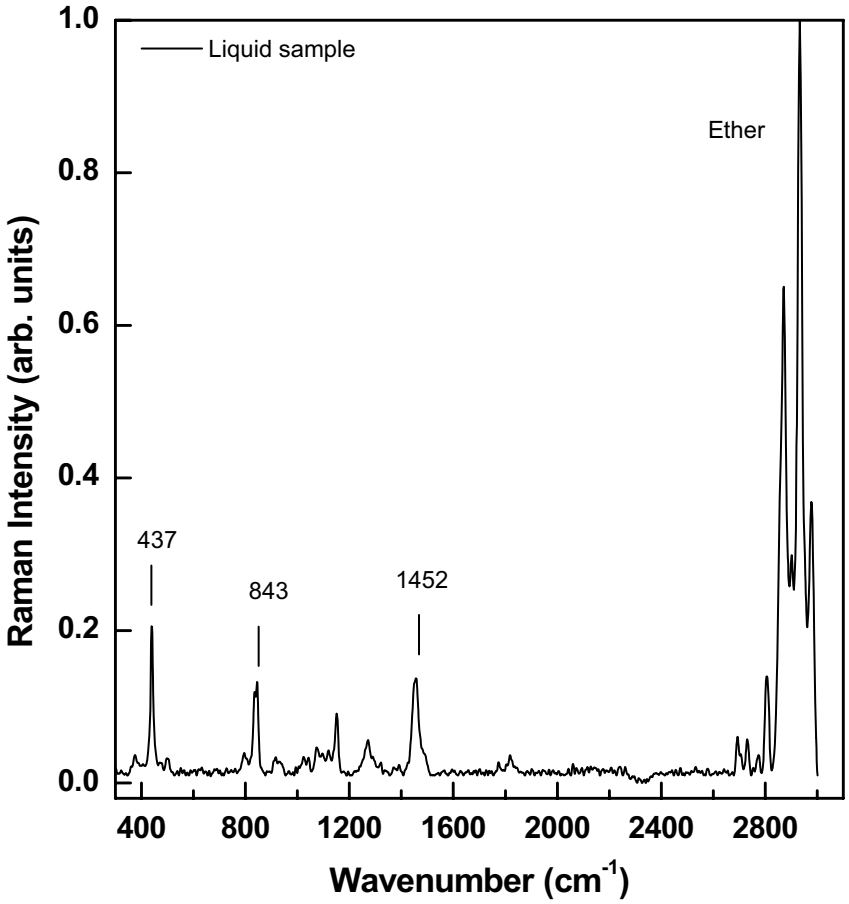

Figure 14. Raman spectra of alane in liquid form. 1st prepration method.

In addition, given the fact the most intense vibrations in the previous sample were assigned to both the precursor and the solvent, two additional filtering and washing procedures were performed on the sample. Therefore, the Raman spectra shown in Figure 15 correspond to the sample immediately after two filtering procedures (black line) and after a longer time of atmospheric exposure (blue line).

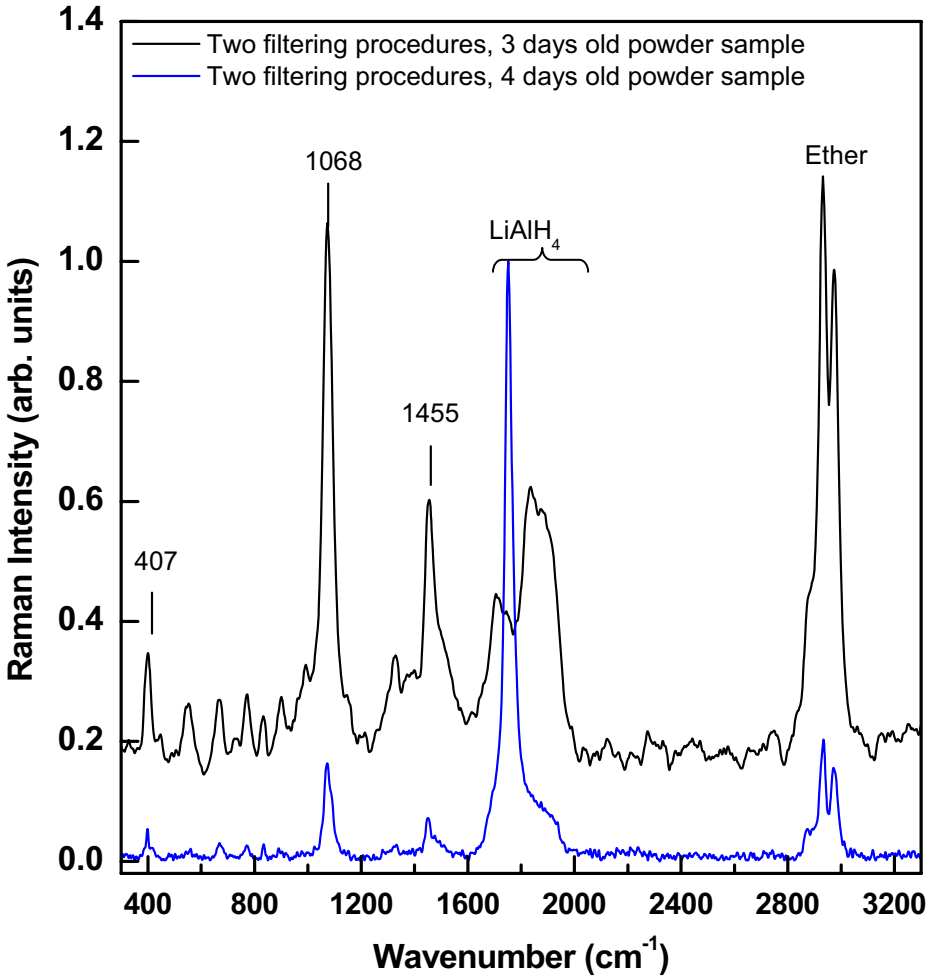

Figure 15. Raman spectra of filtered samples after 3 (black) and 4 (blue) days after synthesis. 1st preparation method.

The existence of diethyl ether solvent vibrational lines are still observed in both these Raman spectra. For example, the spectrum of the sample exposed for three days to the atmosphere (black line) contains ether vibrations at 407 cm^{-1}, 2935 cm^{-1}, and 2975 cm^{-1}. The spectrum of the sample that had been exposed to the atmosphere for four days (blue line) contains only the ether vibrations at 2935 cm^{-1}

and 2968 cm^{-1}. Also, both spectra contain vibrations due to the $LiAlH_4$ precursor: at 1843 cm^{-1} in the black line spectrum and at 1750 cm^{-1} in the blue line spectrum. Even after heating, the peak at 1455 cm^{-1} could be seen in both of these Raman spectra. However, in contrast to the spectrum shown in Figure 14, there is a new vibration present in both samples at 1068 cm^{-1}, which according to Kato *et al.*[20] corresponds to γ-AlH_3.

To fully determine the effects of the heat treatment, as well as that of the two additional filtering procedures, which could influence the expected decomposition of the sample, let us plot in Figure 16 and further analyze the combined Raman spectra of these three samples. Spectrum 16(a) (black line) represents the freshly synthesized liquid aluminum hydride sample that has not been exposed to the atmosphere. Spectra 16(b) (blue line) and 16(c) (red line) represent the aluminum hydride sample after 3 and 4 days of atmospheric exposure, respectively. A vertical translation of these spectra was performed for clarity

From a direct comparison of these spectra, two important observations can be made. First, a marked decrease of the vibrations at 2860 cm^{-1}, 2923 cm^{-1}, and 2980 cm^{-1} occurs for the spectrum of the samples that were filtered and washed twice, especially for the spectrum in red. Also, the diethyl ether vibrations at 439 cm^{-1} and 844 cm^{-1} in the black line spectrum completely disappear in the red line spectrum; this effect is marked by black arrows. Second, a new vibration at 1068 cm^{-1} appears for the samples that were heated and filtered. As previously mentioned, this vibration is assigned to a new polymorph of aluminum hydride, γ-AlH_3.

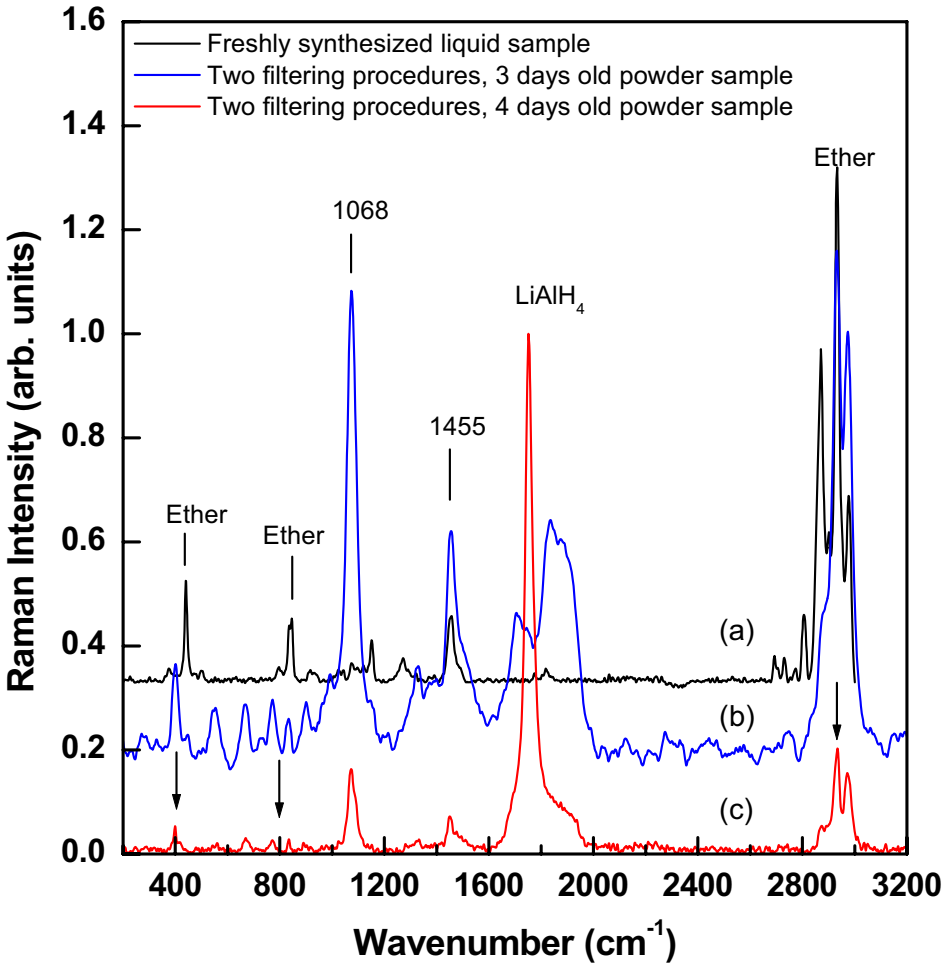

Figure 16. Comparison of Raman spectra of (a) unfiltered (black) and filtered samples after (b) 3 days (blue) and (c) 4 days (red). 1st preparation method.

Then, the fact that the vibrations arising due to the ether solvent drastically decrease or completely disappear with the filtering procedures tells us that the solvent evaporates with time. This, in conjunction with the appearance of the vibration at 1068 cm^{-1}, which is assigned to γ-AlH_3, allows us to unambiguously assign the vibration at 1455 cm^{-1} to this new alane polymorph.

Next, let us analyze the sample synthesized by the method described in section 2.1.2. The spectrum of this sample before any filtering procedures is presented in Figure 17.

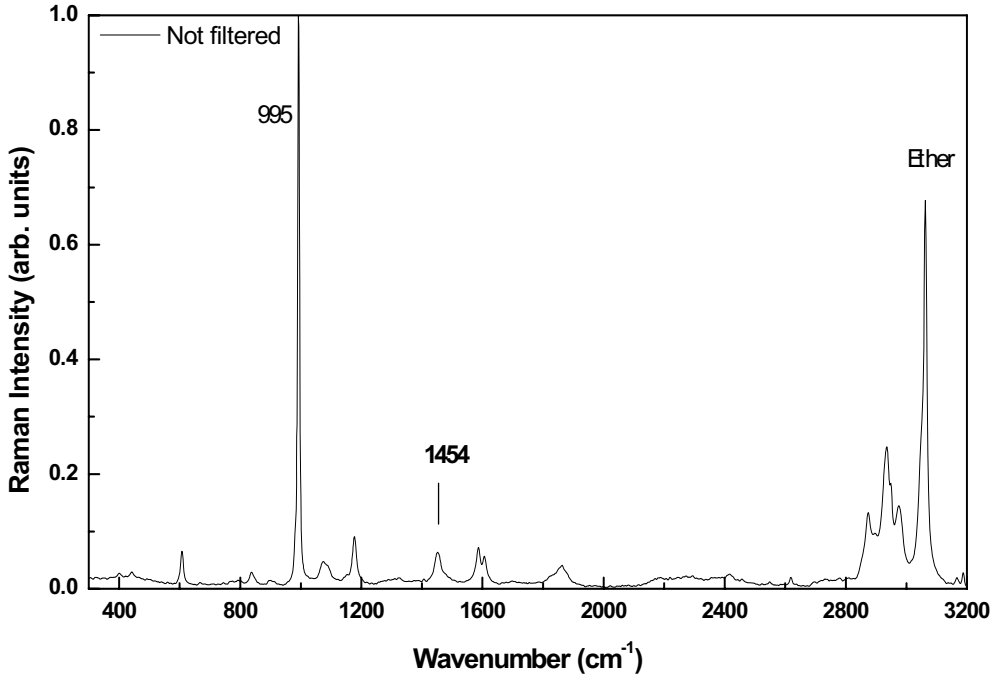

Figure 17. Raman spectra of unfiltered sample. 2nd preparation method.

The most intense peak in this Raman spectrum, at 995 cm^{-1}, corresponds to one of the benzene solvent used for this sample preparation. Also, there is a small vibration at 1454 cm^{-1}, that according to Kato *et al.*[20] is evidence of alane's presence. The vibrations at 2874 cm^{-1}, 2930 cm^{-1}, and 3065 cm^{-1} are attributed to the other solvent, diethyl ether. As previously, we are going to investigate the vibrational changes of this sample after two washings, two filtering procedures, and after

significant atmospheric exposure (three days). The corresponding Raman spectra are presented in Figure 18.

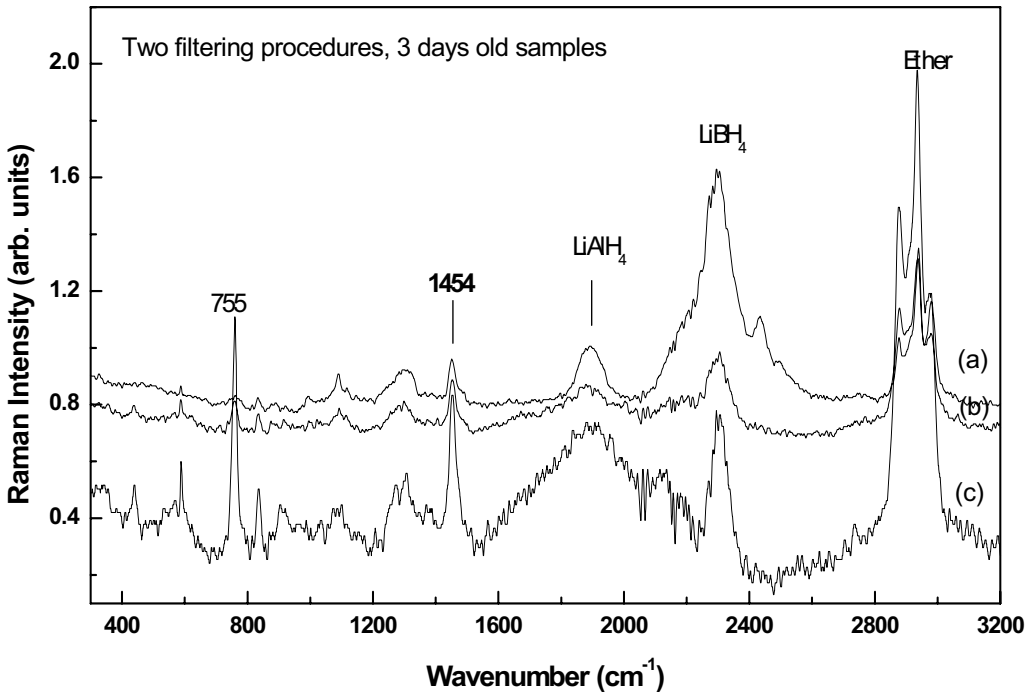

Figure 18. Raman spectra of filtered samples from (a) least to (c) greatest atmospheric exposure. 2nd preparation method.

The spectrum 18 (a) represents the least amount of atmospheric exposure and 18 (c) the greatest. Again, the most intense vibrations at 2871 cm^{-1}, 2937 cm^{-1}, and 2982 cm^{-1} are due to the diethyl ether solvent. The other precursors employed are present as well. The vibration at 2305 cm^{-1} corresponds to $LiBH_4$, while the vibration at 1890 cm^{-1} corresponds to $LiAlH_4$. The vibration at 1454 cm^{-1} suggests the presence of alane in all three spectra. The spectrum of the sample with the greatest atmospheric exposure (18(c)) contains an additional peak at 755 cm^{-1}.

According to Wong *et al* [31] and Tkacz *et al* [32] it could be assigned to α-AlH_3; however, given its intensity and its absence in previous spectra, it most likely corresponds to one of the precursors.

Figure 19 below presents the Raman spectra of both the unfiltered and twice filtered samples. This allows us to compare and determine the exact effects that washing and atmospheric exposure have on the sample prepared by this method.

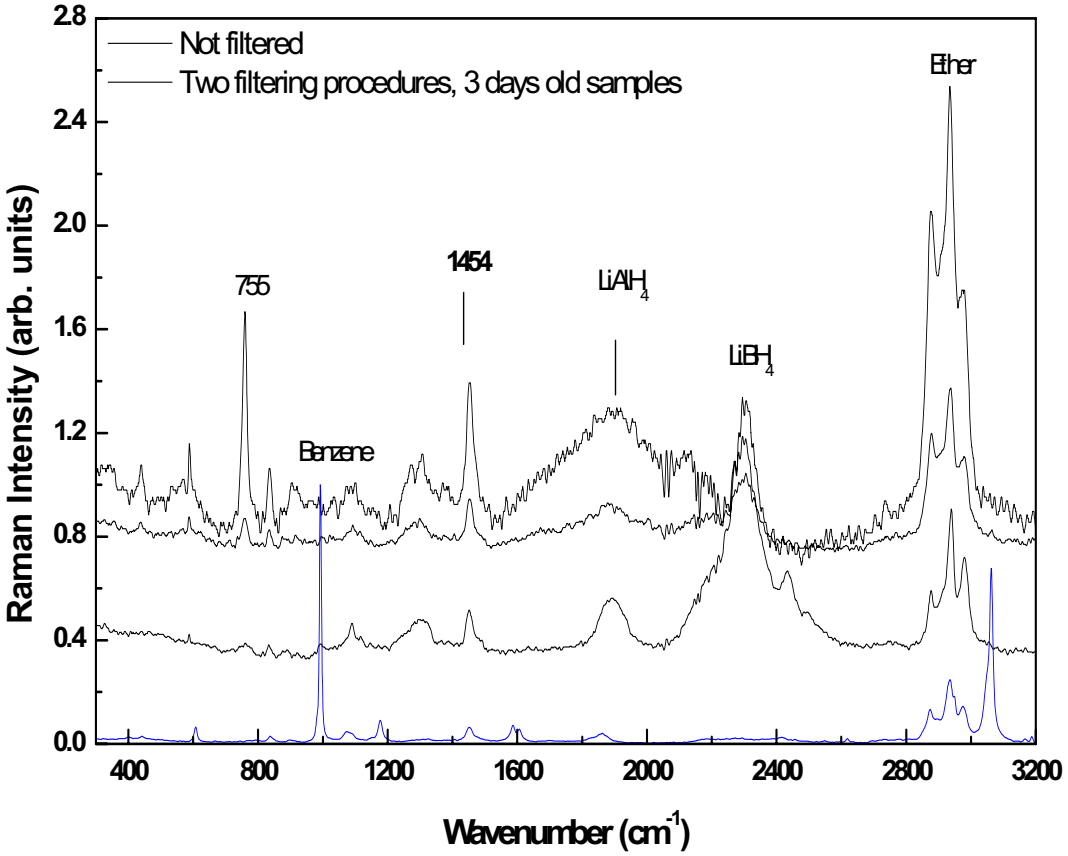

Figure 19. Comparison of Raman spectra of unfiltered (blue) and filtered samples (black) at different atmospheric exposure times. 2nd preparation method.

A glance at these spectra reveals that for this sample preparation method, the two additional filtering procedures do not contribute to the elimination of diethyl ether solvent, as was the case for the first method. The vibrations in the region of 2850-3000 cm^{-1} are present in all four spectra. However, the other solvent, benzene, does disappear in the samples that were filtered. The vibration at 995 cm^{-1}, which is assigned to benzene, is only present in the unfiltered sample, as seen in the blue line spectrum. The vibrations corresponding to $LiAlH_4$ at 1890 cm^{-1} and $LiBH_4$ at 2305 cm^{-1} are not affected by the filtering procedures. Last, the presence of the vibration at 1454 cm^{-1} corroborates with the presence of γ-AlH_3 in all four samples.

The detailed analysis of the infrared and Raman data obtained for aluminum hydrides prepared by two different chemical preparation methods has provided valuable insights. First, infrared data demonstrate the presence of α-AlH_3 in all these samples. Also, the Al_2O_3 layer formation on the surface of the aluminum hydride after atmospheric exposure is confirmed. Meanwhile, Raman data show the presence of another polymorph of alane, i.e. γ-AlH_3, in the samples synthesized by both methods. Regarding the effectiveness of filtering and washing procedures, both infrared and Raman data confirm that they are only partially successful. In some instances, the solvent(s) can either evaporate and/or be removed by the filtering procedure. However, other precursors, such as $LiBH_4$ and $LiAlH_4$, are not easily removed; even two filtering procedures appear ineffective in removing them.

In conclusion, the two sample preparation procedures employed in this work have been found successful in producing a mixture of aluminum hydride polymorphs, α-AlH_3 and γ-AlH_3. However, no success was achieved in producing pure aluminum hydride, due to two main reasons. One, the precursors employed in the preparation were not easily removed, and second, an aluminum oxide layer was present in all samples. Then, a better chemical synthesis, for an effective separation of pure alane, needs to be employed.

The next section consists in a detailed analysis of computer simulation data.

3.3. Computational analysis of Infrared and Raman vibrational properties

3.3.1 AlH_3 molecule and unit cell

Computational simulation was done with Gaussian 03w[33] to obtain a complete set of information regarding infrared absorption and Raman vibrational properties of the aluminum trihydride molecule and compare it with previous theoretical and experimental studies. In particular, density functional theory (DFT) calculations were performed for which the 6-311 + G basis set and a B3LYP density functional were employed. In a study conducted by Curtis *et al.*[34], it was determined that the use of B3LYP/6-311+G zero point energies and geometries for the calculation of vibrational frequencies gives the best agreement with experimental data.

On the other hand, since even a slight change in either the angle or length of the unit cell parameters affects the outcome of any simulation, we will proceed to describe the exact parameters used in this work. The crystal structure of the most stable hydride, α-AlH_3, was modeled after the first thorough description made by Turley *et al.*[7]. Our alane unit cell was first created in Cerius software and then imported to GaussView 3.09 [35] for complete analysis. A hexagonal crystal structure with a=4.94Å, c=11.80Å, α=56.1° and composed of alternating planes of Al and H atoms with respect to the z-direction (spaced a distance of z/12 or 0.98 Å) was used. This structure, belonging to the $R\bar{3}c$ space group, has for, the *(x,y,z)* positions of the main atoms, Al:(0, 0, 0) and H:(0.628, 0, 0.250). Each of the Al atoms is surrounded by six H atoms, three in the plane above and three in the plane below.

The octahedral arrangement of H atoms forms Al-H-Al bridges of 1.715 Å at an angle of approximately 141.2° [7]. In addition, the average distance between the H atoms located in different planes was approximated as 2.42 Å. An average of 3.24 Å for the distance between Al atoms was used. Along the c-plane, Al atoms are arranged in columns at intervals of c/2. Each unit cell is composed of three of these columns, with Al atoms at z= 0 and $^{6}/_{12}$, z= $^{2}/_{12}$ and $^{8}/_{12}$, and z= $^{4}/_{12}$ and $^{10}/_{12}$. Hydrogen atoms are arranged in spirals along the c-plane and at intervals of c/3. Six of these spirals are present in each unit cell, with three H atoms at $^{3}/_{12}$, $^{7}/_{12}$, and $^{11}/_{12}$ and three at z= $^{1}/_{12}$, $^{5}/_{12}$, and $^{9}/_{12}$. A side and a top view of the unit cell are presented in Figure 20 for visualization of the twelve layers or the hexagonal arrangement, respectively.

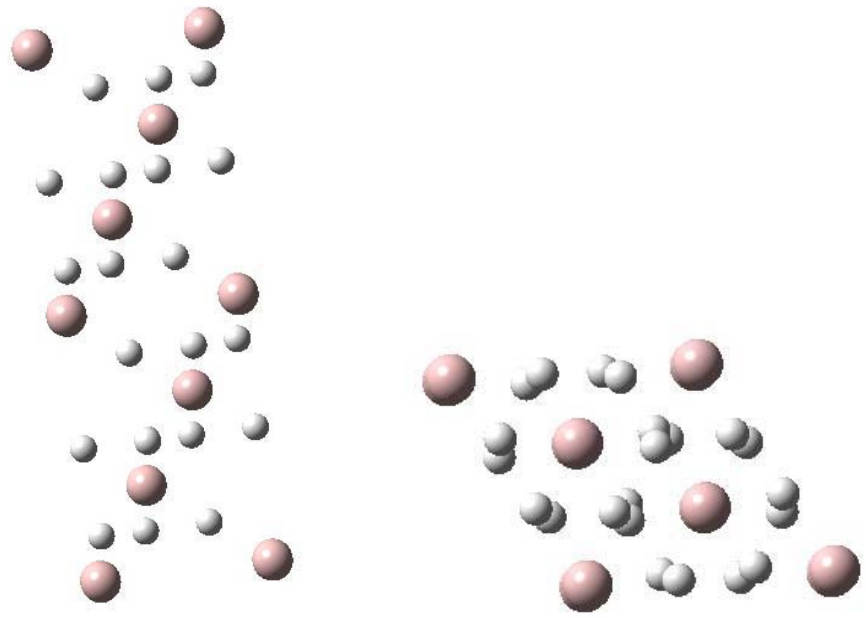

Figure 20. Side and top view of α-AlH_3.

The infrared absorption and Raman simulated results with no scaling factor, as suggested by Curtis *et al.*[34], are presented in Figures 21 and 22, respectively. The main vibrations of α-AlH_3 are identified by red lines. An expected difference between computed and experimental vibrational lines of α-AlH_3 is observed, mainly due to consideration of a single unit cell and neglect of periodical arrangement of unit cells existent in any material. Only the major frequencies of the simulated spectrum were further considered for analysis.

A summary of the current simulated infrared absorption and Raman data and of previous published experimental and simulated results is presented Tables 2 and 3, respectively. The current computed results match within a good range the experimental spectroscopic data obtained by Chertihin *et al.*[15] and Wang *et al.* [16] on

samples synthesized by laser ablation, and by Wong *et al.* [31] on samples prepared using a chemical approach.

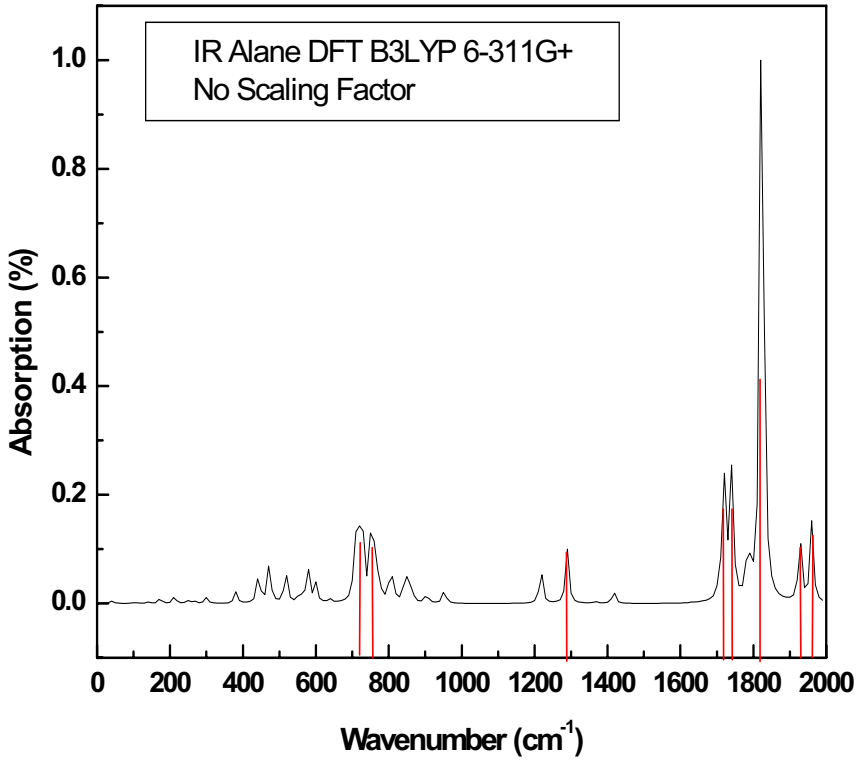

Figure 21. Simulated infrared absorption data for the unit cell of alane.

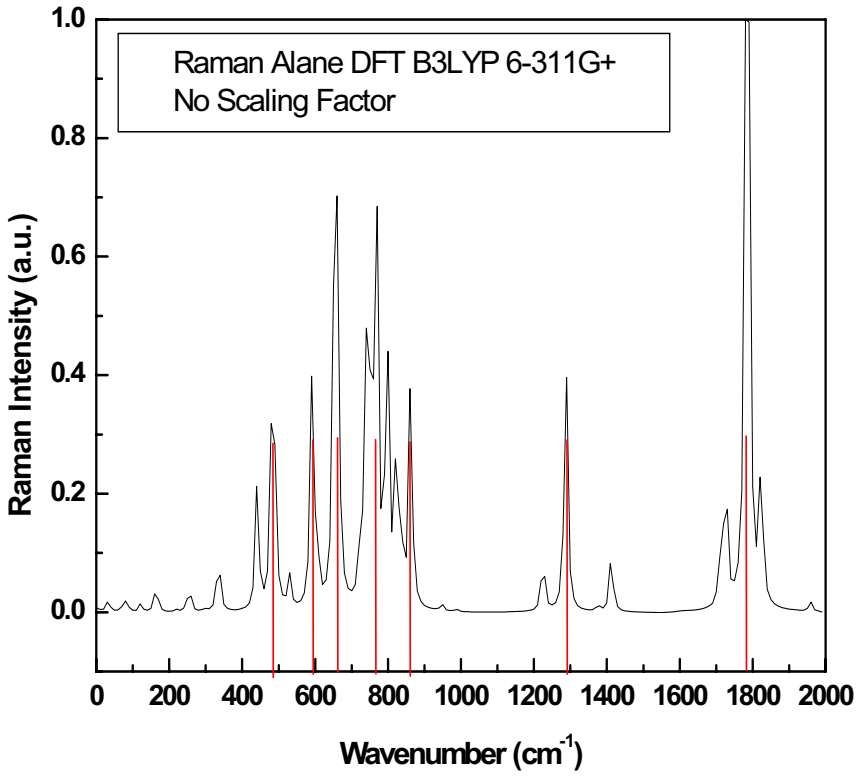

Figure 22. Simulated Raman data for the unit cell of alane.

This is not the case for the study by Matzek *et al.*[12], where the presence of solvent excess on the etherated sample might have lead to a modification of vibrational properties as compared with the non-solvated sample synthesized by Wong *et al.*[31]. Also, comparison between our current simulated data and the ones reported in the literature shows good agreement only for the case of Wang *et al.*[16], where a DFT method and a slightly different basis set B3LYP/6-311++G** were used.

Although the present theoretical predictions produce extra vibrational lines as compared with reported experimental Raman results, the current simulated data

match the first three and most dominant vibrations. While for the most important vibrations, agreement with earlier works is obtained both experimentally and theoretically, a difference of about 250 wavenumbers occurs for the last two vibrations in the higher frequency range.

Table 2 - Infrared Vibrations of α-AlH_3

Laser Ablation[15]	Laser Ablation[16]	Laser Ablation[16]	Chemistry[12]	Chemistry[31]	Ab initio MBPT[15]	DFT B3LYP[16]	DFT LDA[36]	DFT VASP[30]	Present Work
							286		
							293	311	
							512		
							583	560	
			640				635	632	
697.9	711.3	720	680		745.6	713.1	777		724.9
783.4	777.9			824	823	799.4			754.7
			870				851	858	
			955						
			1020				1008		
				1241					1289.5
		1720	1650	1679			1650	1718	1721.9
			1760				1687	1750	1740.9
				1842			1833		1823.3
1882.8	1883.7					1939.1	1836		1927.7
					2014.1	1948.7			1960.3

Table 3 - Raman Vibrations of α-AlH_3

INS[37]	Chemistry[31]	Chemistry[12]	DFT LDA [36]	DFT VASP[30]	Present Work
510.3	512.9	512.0	490.0	497.0	484.7
					590.2
					661.2
712.8	724.1	723.0		738.0	766.9
850.5	856.8	849.0	812.0		861.7
1037.0	1045.0	1043.0	993.0	1034.0	
					1288
		1501.0	1481.0	1520.0	
					1784.8

Since the main objective of these computational results is to predict the vibrations for the new Al_4H_6 aluminum hydride complex, where the crystalline structure and, consequently, the unit cell parameters are unknown, a good method would be to compare the vibrational data obtained from modeling a single α-AlH_3 molecule with those from an α-AlH_3 unit cell simulation.

The infrared absorption and Raman data for a single planar molecule of α-AlH_3 are shown in Figure 23. Also, for convenience, we list in Tables 4 and 5 the computed results for both, the α-AlH_3 unit cell and the single molecule. There are only three vibrations in the case of α-AlH_3 single molecule simulation, as expected, since only a few atoms interact with each other, and thus, only a few allowed vibrations are possible. Nevertheless, the three infrared absorption vibrations obtained do match the experimental results of Wong *et al.*[31], where chemically synthesized samples were analyzed.

Table 4. Comparison of Infrared Data- AlH_3

Unit	Molecule
724.9	
754.7	755.5
	812.1
1289.5	
1721.9	1685.2
1740.9	
1823.3	
1927.7	
1960.3	

Table 5. Comparison of Raman Data -AlH_3

Unit	Molecule
484.7	
590.2	
661.2	
766.9	
861.7	812.1
1288	
1784.8	1674.9

While the first vibration in the computed Raman data matches all previous results, the second one comes much closer to the earlier predicted vibration at about 1500 wavenumbers than the one obtained for the unit cell.

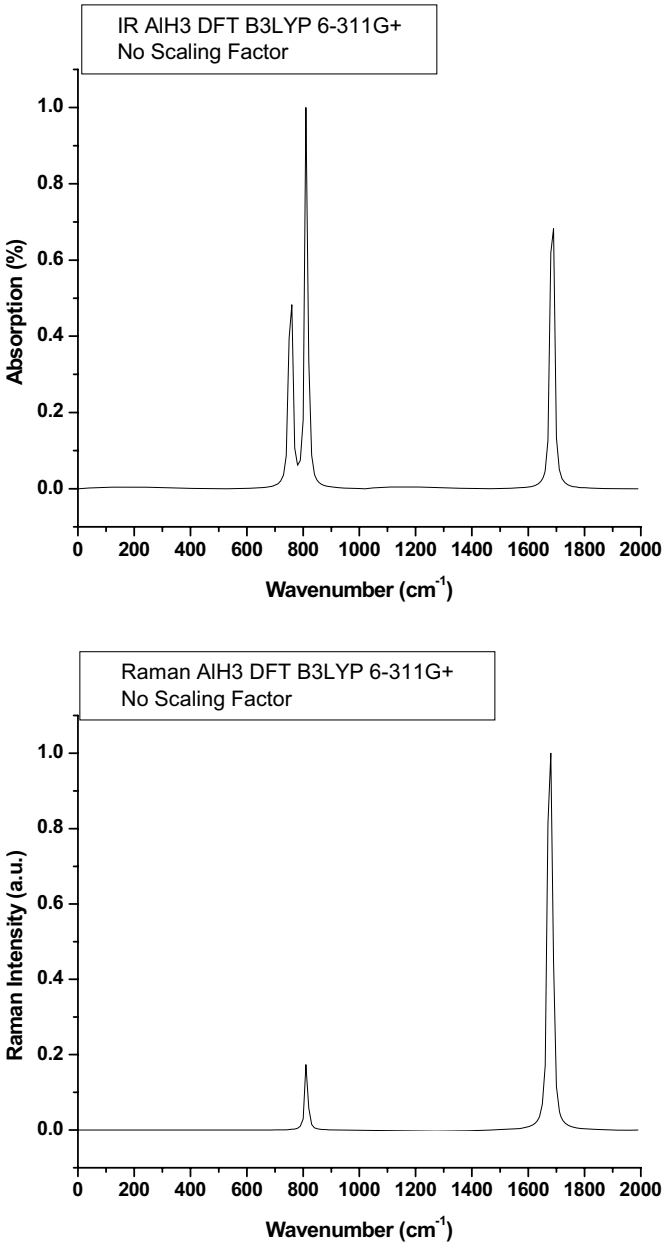

Figure 23. Simulated Infrared and Raman data for a single molecule of α-AlH_3.

Also, it is worth noting that these results were obtained for a single planar molecule. However, there is no planarity in the structure for the building block in the unit cell. In the latter, aluminum and hydrogen form distorted tetrahedrons where the hydrogen atoms are not in a planar state. Thus, the next step would consist of modeling a single molecule that better represents the structural arrangement of the atoms in the actual material.

In conclusion, while the simulated data for the unit cell is in good agreement with previous experimental and theoretical results, the results are not able to account for all the observed vibrations. Therefore, more attempts are necessary to improve the simulation data as mentioned before.

3.3.2 Al_4H_6 molecule

Now that we have a complete set of simulation data for AlH_3, both for a single molecule and for a unit cell, let us next examine the results obtained for the more energetic Al_4H_6. The figure below represents the molecular structure used for our simulation purposes, where the bond lengths and angles employed are the same as those obtained from theoretical calculations by Li *et al.*[17] for the lowest energy configuration.

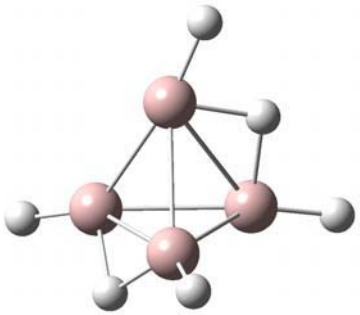

Figure 24. Structure of Al_4H_6 used for Gaussian simulations.

The same theoretical method and basis set previously used for AlH_3 were employed for this molecule. The Infrared and Raman simulation spectra are shown below.

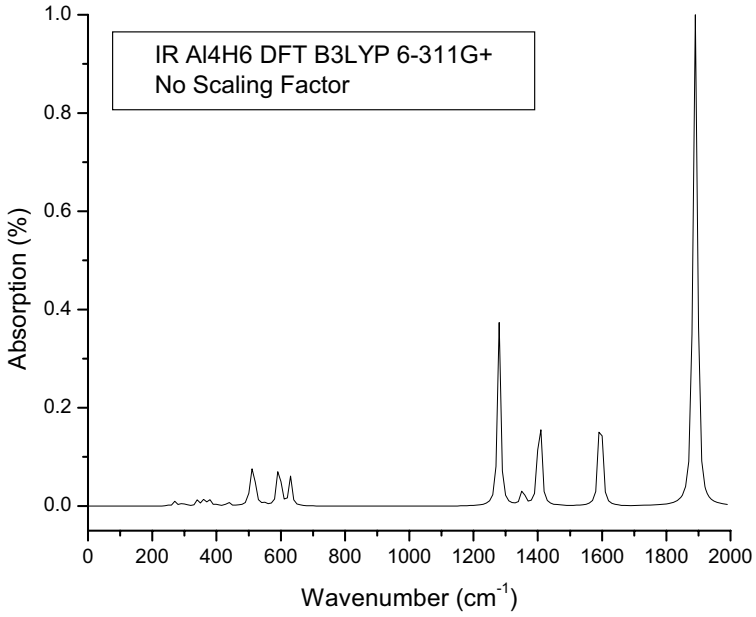

Figure 25. Simulated Infrared data for a single molecule of Al_4H_6.

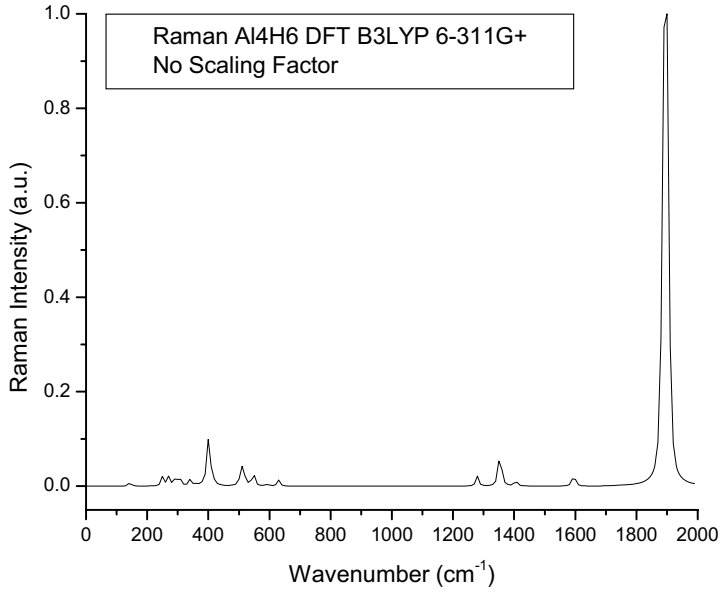

Figure 26. Simulated Raman data for a single molecule of Al_4H_6.

In contrast to the results obtained for the AlH_3 molecule, there are more vibrations present in the spectra of this new molecule due to the presence of more atoms. Also, as expected, the vibrations of Al_4H_6 are completely different from those of AlH_3. Tables 6 and 7 shown below contain the results obtained for both AlH_3 and Al_4H_6 for better comparison.

Table 6. Comparison of Infrared Data- Al_4H_6

Al_4H_6	AlH_3
507.8	
594.1	
629.58	
	755.5
	812.1
1279.6	
1405.8	
1594.9	
	1685.2
1886.9	

Table 7. Comparison of Raman Data -Al_4H_6

Al_4H_6	AlH_3
398.9	
507.8	
	812.1
1353.9	
	1674.9
1902.1	

These results can serve as a basic reference for future attempts at synthesizing and identifying the more energetic aluminum hydride, Al_4H_6. However, similar to the AlH_3 scenario, where the theoretical spectrum of a single molecule does not account for all the vibrations present in both the simulated spectrum of a unit cell or the experimental results; the spectra shown in figures 25 and 26 represent only an approximation. Also, to the best of the author's knowledge, these results represent the first theoretical spectroscopic calculations performed for this new molecule. Then, future efforts would consist in attempting to simulate the structure and vibrational properties of a unit cell for Al_4H_6.

Chapter 4

Conclusions

4.1 Concluding Remarks

After a thorough examination of two different synthesis processes as well as experimental and theoretical spectroscopic studies of aluminum hydride, an energetic material suited for rocket fuel and hydrogen storage applications, we have arrived at several important conclusions. For the purpose of this thesis, aluminum hydride was synthesized following two different procedures. First, non-solvated α-AlH_3 was synthesized by following the method of Brower *et al.*[11] and Schmidt *et al.*[4]. The second procedure consisted of a method modeled after that employed by both Brower *et al.*[11] and Petrie *et al.*[13] where the end results were α-AlH_3 crystals.

There are various phenomena revealed by the FT-IR data. First, the sensitivity of the sample to atmospheric effects is observed as a broadening of the water absorption band as exposure time increases. Second, the solvent present in the samples evaporates with greater time exposure as seen by either the decrease or disappearance of its vibrational lines. Third, one of the precursors, $LiBH_4$, is successfully removed by the washing procedures, as seen by the disappearance of its vibrational features for the case of the sample synthesized by the first method discussed.

Most important, the FT-IR data confirm the presence of various vibrational features that are characteristic of the stable α-AlH_3 phase in samples synthesized by both procedures. In addition, the presence of Al_2O_3 is also established in samples obtained from both methods, but this was anticipated, since the presence of an oxidation layer as a stabilizer is expected. In conclusion, FT-IR data confirm the chemical synthesis of alane in conjunction with a protective oxide layer.

Similarly to the data obtained from FT-IR measurements, the Raman data confirm the disappearance of the vibrational lines corresponding to one of the solvents, ether, after filtering procedures for the sample obtained by the first method. On the other hand, in the second procedure two solvents were used. In this case, the two additional filtering procedures do not contribute to the elimination of one of the solvents, ether, as was the case for the first method. However, the vibrational lines corresponding to the other solvent, benzene, do disappear in the samples that are filtered. Also, contrary to the samples synthesized by the first method, the vibrations corresponding to $LiAlH_4$ and $LiBH_4$ are not affected by the filtering procedures.

Regarding aluminum hydride, Raman data show the presence of some of the vibrational lines characteristic of α-AlH_3 in samples prepared by both methods. Another significant discovery is the presence of two vibrational lines at 1068 and 1454 cm^{-1} that are characteristic of a different aluminum hydride phase, namely γ-

AlH_3, in the Raman spectrum of samples prepared by both chemical synthesis methods.

Then, both Infrared and Raman data confirm that the filtering and washing procedures are only partially successful. The solvents either evaporate or are removed by the washing procedure. Nevertheless, the vibrational lines of other precursors, specifically $LiBH_4$ and $LiAlH_4$, are still present in the different spectra even after two filtering procedures.

Finally, the two chemical synthesis procedures described in this thesis were successful in preparing a mixture of aluminum hydride polymorphs, specifically α-AlH_3 and γ-AlH_3. Still, the samples obtained were not impurity free. Some of the precursors were still present in the samples, and most notably, an aluminum oxide layer is present in all samples. Thus, a method for effective separation of pure alane needs to be developed.

In addition to the experimental spectroscopic analysis present in this thesis, a thorough theoretical investigation was performed for the spectroscopic characteristics of α-AlH_3 and Al_4H_6. First, computer simulations of the Infrared and Raman spectra of the unit cell of the stable α-AlH_3 are compared to other experimental and theoretical results obtained in peer-reviewed publications. Then, computer simulations for a single AlH_3 molecule were performed and compared against the results obtained for a single unit cell. The simulated data for the unit cell is in good agreement with previous work, which is also the case for the data for a single molecule. However, in the latter case the results are not able to account for

all the observed vibrations. Last, a theoretical investigation of the spectroscopic characteristics of Al_4H_6 was presented. The simulated data is only valid for a single molecule of this new energetic material since no information is available at the moment for its unit cell structure.

4.2 Future Work

Although the chemical methods employed for the purpose of this thesis were adapted from work previously reported in the literature, we were not successful in synthesizing an impurity free aluminum hydride sample. Thus, future work would include finding methods for successful chemical separation of the different aluminum hydride phases from precursors and solvents, while eliminating the decomposition and oxidation observed as a result of the filtering and washing procedures used in this work. Also, new ways of synthesizing the more energetic and interesting aluminum hydride, Al_4H_6, need to be thoroughly investigated.

Regarding theoretical investigations, while the simulated data are in good agreement with previous results, they do not account for all the observed vibrations; then, the next step would consist in modeling a single molecule that most closely matches the structural arrangement inside a unit cell of the actual material. This will allow us to obtain simulation data that better matches experimental results.

In addition, future efforts would consist in attempting to improve the computational simulations of the vibrational properties of Al_4H_6. Given that the results obtained from simulations are very sensitive to values of the bond lengths and angles between the various atoms, investigating the effects of these parameters for the case of this new molecule could provide valuable information.

Also, as mentioned previously, the structure used for these simulations was obtained from theoretical calculations by Li *et al.*[17], where the lowest energy configuration was assumed. Then, given that this structure remains an approximation at best, it would be advantageous to delve deeper into the calculations performed to obtain this structure and determine if other variations are feasible as well. The end goal is to calculate the theoretical vibrational properties of Al_4H_6 not only as a single molecule, but also in a unit cell configuration which would allow us to calculate infrared and Raman spectra that can serve as references for future analysis of aluminum hydrides.

References

[1] J. Maehlen, V. Yartis, R. Denys, M. Fichtner, C. Frommen, B. Bulychev, P. Pattison, H. Emerich, Y. Filinchuck, and D. Cheryshov, *J. Alloys and Compounds* **446**, p. 280 (2007).

[2] L. DeLuca, L. Galfetti, F. Severini, L. Rosettini, L. Meda, G. Marra, B. D'Andrea, V. Weiser, M. Calabro, A. Vrozhtsov, A. Glazunov, and G. Pavlovets, *Aerospace Science and Tech.* **11**, p. 18 (2007).

[3] T. Bazyn, R. Eyer, H. Krier, and N. Glumack, *J. of Propulsion and Power* **20**, no.3, p. 427 (2004)

[4] D. L. Schmidt, C. B. Roberts, P. F. Reigler, M. F. Lemanski Jr, and E. P. Schram, *Inorganic Syntheses* **vol 14**, p. 47 (1973).

[5] X. Ke, A. Kuwabora, and I. Tanata, *Phys. Rev. B* **71,** p. 184107 (2005).

[6] J. Ismail, and T. Hawkins, *Thermochimica Acta* **439,** p.32 (2005).

[7] J. Turley, and H. Rinn, *Inorg. Chem.* **8**, no. 1, p. 18 (1969).

[8] V. Yartys, R. Denys, J. Maehlen, C. Frommen, M. Fichtner, B. Bulychev, and H. Emerich, *Inorg. Chem.* **46**, no. 4, p. 1051 (2007).

[9] J. Graetz, S. Chaudhuri, Y. Lee, T. Vogt, J. Muckerman, and J. Reilly, *Phys. Rev. B* **74**, p. 214114-1 (2006)

[10] A. Finholt, A. Bond, and H. Schlesinger, *J. Am. Chem. Soc.* **69**, p. 1199 (1947).

[11] F. M. Brower, N. E. Matzek, P. F. Reigler, H. W. Rinn, C. B. Roberts, D. L. Schmidt, J. A. Snover, and K. Terada, *J. Am. Chem. Soc.* **98**, p. 2450 (1976).

[12] N. Matzek, and D. Musinski, *Aluminum Hydride*, Patent No. US 3 883 644, (1975).

[13] M. Petrie, J. Bottaro, R. Schmitt, P. Penwell, D. Bomberger, *Stabilized aluminum hydride polymorphs*, Patent No. US 6 617 064, (2003).

[14] M. Appel, and J. Frankel, *J. Chem. Phys.* **42**, no. 11, p. 3984 (1965)

[15] G. Chertihin and L. Andrews, *J. Phys. Chem.* **97**, p. 10297 (1993)

[16] X. Wang, L/ Andrews, S. Tam, M. DeRose, and M. Fajardo, *J. Am. Chem. Soc.* **125**, p. 9218 (2003)

[17] X. Li, A. Grubisic, S. Stokes, J. Cordes, G. Gantefor, K. Bowen, B. Kiran, M. Willis, P. Jena, R. Burgert, and H. Schnockel, *Science* **315**, p. 356 (2007).

[18] B. Rao, P. Jena, S. Burkart, G. Gantefor, and G. Seifert, *Phys. Rev. Lett.* **86,** no. 4, p. 692 (2001)

[19] G. Sandrock, J. Reilly, J. Graetz, W. Zhou, J. Johnson, and J. Wogrzyn, *App. Phys. A* **80,** p. 687 (2005).

[20]T. Kato, Y. Nakamori, S. Orimo, C. Brown, and C. Jensen, *J. of Alloys and Compounds* **446-447**, p. 276 (2007)

[21] P. R. Griffiths, and J. A. de Haseth, *"Fourier Transform Infrared Spectrometry",* 2nd ed., John Wiley & Sons, Inc. Publication, New Jersey, (2007).

[22] N. B. Colthup, L. H. Daly, and S. E. Wiberley, *"Introduction to Infrared and Raman Spectroscopy",* 3rd ed., Academic Press Inc., San Diego, (1990).

[23] http://scienceworld.wolfram.com/physics/MichelsonInterferometer.html

[24] http://mmrc.caltech.edu/mmrc_html/FTIR/FTIRintro.pdf

[25] R. J. Bell, "*Introductory Fourier Transform Spectroscopy*", Academic press, New York, (1972).

[26] J. Ferraro, K. Nakamoto, C. Brown, "*Introductory Raman Spectroscopy",* 2nd ed., Academic Press Inc., San Diego, (2003)

[27] http://www.kosi.com/raman/resources/tutorial/index.html

[28] B. Smith, "*Fourier Transform Infrared Spectroscopy",* CRC Press, Boca Raton, (1996)

[29] Courtesy of Bruker Inc.

[30] Y. Wang, J. Yan, and M. Chou, *Phys. Rev. B.* **77**, p. 014101 (2008)

[31] C. Wong and P. Miller, J. *Ener. Mater.s* **23**, p. 169 (2005).

[32] M. Tkacz, T. Palasyuk, J. Graetz, and S. Saxena, *J. Raman Spectrosc.* DOI: 10.1002/jrs (2008)

[33] Gaussian 03, Revision D.01, M. J. Frisch, G. W. Trucks, H. B. Schlegel, G. E. Scuseria, M. A. Robb, J. R. Cheeseman, J. A. Montgomery, Jr., T. Vreven, K. N. Kudin, J. C. Burant, J. M. Millam, S. S. Iyengar, J. Tomasi, V. Barone, B. Mennucci, M. Cossi, G. Scalmani, N. Rega, G. A. Petersson, H. Nakatsuji, M. Hada, M. Ehara, K. Toyota, R. Fukuda, J. Hasegawa, M. Ishida, T. Nakajima, Y. Honda, O. Kitao, H. Nakai, M. Klene, X. Li, J. E. Knox, H. P. Hratchian, J. B. Cross, V. Bakken, C. Adamo, J. Jaramillo, R. Gomperts, R. E. Stratmann, O. Yazyev, A. J. Austin, R. Cammi, C. Pomelli, J. W. Ochterski, P. Y. Ayala, K. Morokuma, G. A.

Voth, P. Salvador, J. J. Dannenberg, V. G. Zakrzewski, S. Dapprich, A. D. Daniels, M. C. Strain, O. Farkas, D. K. Malick, A. D. Rabuck, K. Raghavachari, J. B. Foresman, J. V. Ortiz, Q. Cui, A. G. Baboul, S. Clifford, J. Cioslowski, B. B. Stefanov, G. Liu, A. Liashenko, P. Piskorz, I. Komaromi, R. L. Martin, D. J. Fox, T. Keith, M. A. Al-Laham, C. Y. Peng, A. Nanayakkara, M. Challacombe, P. M. W. Gill, B. Johnson, W. Chen, M. W. Wong, C. Gonzalez, and J. A. Pople, Gaussian, Inc., Wallingford CT, 2004.

[34] L. Curtis, K. Raghavachari, P. Redfern, and J. Pople, *Chem. Phys. Letters* **270**, p. 419 (1997).

[35] GaussView, Version 3.09, Roy Dennington II, Todd Keith, John Millam, Ken Eppinnett, W. Lee Hovell, and Ray Gilliland, Semichem, Inc., Shawnee Mission, KS, 2003.

[36] C. Wolverton, V. Ozolins, M. Asta, Phys. Rev. B 69, p. 144109 (2004)

[37] A. Kolesnikov, M. Adams, V. Antonov, N. Chirin, E. Goremychkin, G. Inkhova, Y. Markushkin, M. Prager, and I. Sahin, J. Phys. Condens. Matter. 8, p. 2529 (1996)

Curriculum Vita

Layra Reza was born in Cd. Juarez, Mexico; the youngest daughter of Roberto Reza and Lucia Villegas. In 2002, she enrolled in El Paso Community College. She transferred to the University of Texas at El Paso during the summer of 2004. In 2005, she received the prestigious MARC fellowship that allowed her to do research with Dr. Felicia Manciu. As an undergraduate she completed three summer internships at the University of California at Santa Cruz, University of Colorado at Boulder, and at Argonne National Laboratory. Moreover, she co-authored a peer reviewed article during her senior year. In addition, she participated in various national American Physical Society meetings, where she presented both oral and poster presentations. After receiving her bachelor's of science degree in Physics she started her graduate studies at the University of Washington. During the spring of 2008, she returned to El Paso and started working in Dr. Manciu's lab, but now as a Mechanical Engineering student. During the fall of 2008 she and her advisor received the Robert S. Hyer recognition for exceptional research from the Texas section of the American Physical Society.

Permanent address: 208 Fewel St

El Paso, TX 79902

-----Original Message-----
From: Choudhuri, Ahsan R.
Sent: Thursday, August 27, 2009 1:15 PM
To: Caudillo, Olympia; Manciu, Felicia S.
Subject: FW: PUblic Release Case 09-MDA-4784 THESIS: Aluminum Hydride Compounds: A Theoretical And Experimental Spectroscopic Study (UNCLASSIFIED)

We received public release approval for Ms. Layra Reza's thesis. It now can be submitted to the library. Please add a page with the following statement
DISTRIBUTION STATEMENT A. Approved for public release; distribution is unlimited.
Approved for Public Release
09-MDA-4784 (26 AUG 09)

-----Original Message-----
From: Lehr, Michael CTR MDA/DV [mailto:Michael.Lehr.ctr@mda.mil]
Sent: Thursday, August 27, 2009 1:05 PM
To: Choudhuri, Ahsan R.
Cc: Schwarz, Richard R CIV MDA/DVI; Smith, John G CTR MDA/DV
Subject: FW: PUblic Release Case 09-MDA-4784 THESIS: Aluminum Hydride Compounds: A Theoretical And Experimental Spectroscopic Study (UNCLASSIFIED)

Classification: UNCLASSIFIED
Caveats: FOUO

Ahsan Choudhuri,

See email below. MDA/PA has reviewed for public release the submitted 89-page thesis as requested and have no objection to public release of this material.

DISTRIBUTION STATEMENT A. Approved for public release; distribution is unlimited.

This material should be marked as follows:

Approved for Public Release
09-MDA-4784 (26 AUG 09)

Material cleared for public release can be reused in its original form any time, any place. Any updating, changing or combining of previously cleared material will form a new document that requires the material be re-submitted for a new public release clearance. Please re-submit any new material with the past clearance documentation. A marked copy of the document indicating where new information is placed will help speed the review.

Regards,
Michael Lehr
Public Release Coordinator
MDA/DV
256.450.1890

-----Original Message-----
From: Szkrybalo, Christopher M CIV MDA/PA
Sent: Thursday, August 27, 2009 1:13 PM
To: Lehr, Michael CTR MDA/DV
Subject: PUblic Release Case 09-MDA-4784 THESIS: Aluminum Hydride Compounds: A Theoretical And Experimental Spectroscopic Study (UNCLASSIFIED)

Classification: UNCLASSIFIED
Caveats: NONE
PA
August 26, 2009

MEMORANDUM FOR DIRECTOR FOR ADVANCED TECHNOLOGY

SUBJECT: Public Release Review, Case No: 09-MDA-4784

THESIS: Aluminum Hydride Compounds: A Theoretical and Experimental Spectroscopic Study

We have reviewed for public release the submitted 89-page thesis as requested and have no objection to public release of this material.

DISTRIBUTION STATEMENT A. Approved for public release; distribution is unlimited.

This material should be marked as follows:

Approved for Public Release
09-MDA-4784 (26 AUG 09)

Material cleared for public release can be reused in its original form any time, any place. Any updating, changing or combining of previously cleared material will form a new document that requires the material be re-submitted for a new public release clearance. Please re-submit any new material with the past clearance documentation. A marked copy of the document indicating where new information is placed will help speed the review.

Should you have any questions or require further information, please contact Yashika Archer at 703-695-1603.

RICK LEHNER
Director of Public Affairs
Office of Public Affairs
Classification: UNCLASSIFIED

Caveats: NONE
Classification: UNCLASSIFIED
Caveats: FOUO